

Distribution Agreement in presenting this thesis as a partial fulfillment of the requirements for a degree from Emory University, I hereby grant to Emory University and its agents the non-exclusive license to archive, make accessible, and display my thesis in whole or in part in all forms of media, now or hereafter now, including display on the World Wide Web. I understand that I may select some access restrictions as part of the online submission of this thesis. I retain all ownership rights to the copyright of the thesis. I also retain the right to use in future works (such as articles or books) all or part of this thesis.

Anika Kapur

April 2, 2025

Investigating the Role of JAK/STAT as a Potential Pharmacological Target for Epilepsy

By Anika Kapur

Nicholas Varvel, PhD.

Advisor

Chemistry

Nicholas Varvel, PhD.

Advisor

Richard Himes, PhD.

Committee Member

Tracy McGill, PhD.

Committee Member

2025

Investigating the Role of JAK/STAT as a Potential Pharmacological Target for Epilepsy

By Anika Kapur

Nicholas Varvel, PhD.

Advisor

An abstract of

A thesis submitted to the Faculty of Emory College of Arts and Sciences

of Emory University in partial fulfillment

of the requirements of the degree of

Bachelor of Science with Honors

Chemistry

2025

Abstract

Investigating the Role of JAK/STAT as a Potential Pharmacological Target for Epilepsy

By Anika Kapur

Epilepsy is a prevalent neurological condition characterized by recurrent spontaneous seizures. The efficacy of current pharmacological agents used to treat epilepsy is limited. Hence, there is a need for the identification of new treatment approaches that incorporate diverse pharmacological targets. Daily administration of CP-690,550 (Tofacitinib Citrate), a JAK 3/1 competitive inhibitor, to kainite-induced epileptic mice in the chronic phase decreases seizure severity and frequency that persisted even after the medication was discontinued. In these same mice, epilepsy-associated deficits in spatial memory and working memory were also rescued. Single-nucleus RNA sequencing (RNAseq) from the same study determined that the general observed upregulation of inflammatory markers was driven by STAT3. A complete understanding of which pathways Tofacitinib is suppressing in which specific cell types to produce this anti-inflammatory effect remains unresolved. Here, in this study, we first establish and optimize a model for LPS induction to mimic the inflammatory cellular environment in the epileptic brain. Subsequently, we use the model of LPS induction to probe the exact effects of Tofacitinib on inflammatory mediators in two relevant cells: BV2-hEP2 microglia and THP1 monocytes. *Our hypothesis is that direct inhibition of the JAK/STAT pathway by CP-690,550 reduces the production of inflammatory mediators by microglia and monocytes.* We find a promising trend in Tofacitinib's suppression of LPS-induced IL-6 mRNA in BV2-hEP2 microglia but fail to detect

any statistically significant effects of Tofacitinib on the mRNA levels of any of the screened pro-inflammatory markers within the selected dose range in THP1 monocytes.

Investigating the Role of JAK/STAT as a Potential Pharmacological Target for Epilepsy

By

Anika Kapur

Dr. Nicholas Varvel
Advisor

A thesis submitted to the Faculty of Emory College of Arts and Sciences
of Emory University in partial fulfillment
of the requirements of the degree of
Bachelor of Science with Honors

Chemistry

2025

Table of Contents

Introduction.....	2
Materials and Methods.....	22
Results.....	30
Discussion.....	45
Conclusions and Future Directions.....	52
Limitations.....	54
References.....	55

Investigating the Role of JAK/STAT as a Potential Pharmacological Target for Epilepsy

Anika Kapur

Emory University School of Medicine, Department of Chemical Biology and Pharmacology,
Atlanta GA, 30322, U.S.A

Key Words

Epilepsy, JAK/STAT, JAK3, Inflammation, Microglia, Monocytes, QRT-PCR, western blot, Cytokine signaling, Tofacitinib, IL-6, LPS, BV2

Abbreviations

JAK (Janus Kinase), STAT (Signal Transducer and Activator of Transcription Proteins), RNAseq (Single Nucleotide RNA Sequencing), qRT-PCR (quantitative reverse transcription polymerase chain reaction), LPS (Lipopolysaccharide), IL-6 (Interleukin-6), IL-1 β (Interleukin-1 beta), IL-10 (Interleukin-10) TNF- α (Tumor Necrosis Factor alpha), CCL2 (chemokine ligand 2, chemoattractant protein-1), CCR2 (C-c chemokine receptor type 2). TLR4 (Toll-like receptor 4), IL-1R (Interleukin-1 receptor), DAMPs (Damage-associated molecular patterns), NMDA receptor (N-methyl-D-aspartate receptor), AMPA receptor (alpha-amino-3-hydroxy-5-methyl-4-isoxazolepropionic acid receptors), SRS (Spontaneous recurrent seizures), HMGB1 (High mobility group box 1 protein), Cox-2 (Cyclooxygenase-2), NFKB (Nuclear Factor Kappa B), GABA_A (gamma-aminobutyric acid), GluR2 (Glutamate Receptor 2), BBB (Blood-brain barrier), H-R-D Motif (histidine-arginine-aspartate motif), D-F-G motif (Aspartate-Phenylalanine-Glycine motif), CP-690,550 (Tofacitinib), SOCS (Suppressor of Cytokine Signaling)

1. Introduction

Defining the Disease Burden of Epilepsy

Epilepsy is a neurological disease characterized by spontaneous and recurrent seizures and affects 65 million individuals worldwide.¹ Individuals with epilepsy not only suffer from the seizures themselves but also suffer from various comorbidities including but not limited to depression, anxiety, autism, and cognitive impairment.¹ These comorbidities can affect the patient's quality of life as much as, or even more than the seizures themselves. Importantly, about 30% of patients do not respond to the current available treatment options.¹ Those that are responsive to treatment, must take medication multiple times a day, as no FDA-approved drugs have demonstrated persistent seizure relief.² Hence, there is a need for the identification of new treatment approaches that incorporate diverse pharmacological targets.

Diagnostic criteria for Epilepsy includes the incidence of two or more epileptic seizures, at least 24 hours apart, that lack "any immediate identified cause".³ Alternatively, an epilepsy diagnosis can be warranted by a single "unprovoked" seizure if accompanied by an elevated risk of experiencing a second seizure in the next 10 years.³ Age of onset, the type of seizure, the EEG patterns, along with other epilepsy syndromes, can also contribute to an epilepsy diagnosis and treatment plan.⁴

Differentiating Action Potentials in the Healthy vs Epileptic Brain

Spontaneous and recurrent seizures manifest in acquired epilepsy due to cellular and molecular changes that create hyperexcitable neurons.⁵ In a healthy brain, neurons maintain a negative resting membrane potential of -70 mV ($E_m = E_{in} - E_{out}$) by regulating the concentration of ions entering and leaving the cell via active and passive transport channels, including sodium, potassium, calcium, and chloride ions.^{6,7} ATP hydrolysis-powered membrane pumps and leaky

potassium channels dominate the maintenance of the resting potential.^{6,8} Upon the reception of stimuli, N-type Ca^{2+} channels facilitate calcium influx into the presynaptic neuron's axon terminal.⁹ This triggers the release of excitatory neurotransmitters into the synaptic cleft which bind to dendrite receptors on the postsynaptic neuron.

To understand the subsequent depolarization sequence, glutamate, an excitatory neurotransmitter, can be used as a case study. The binding of glutamate opens ligand-gated sodium and calcium channels on the postsynaptic neuron, such as AMPA and NMDA, causing sodium and calcium ions to enter the cell, increasing the membrane potential.¹⁰ If the stimulus is strong enough and enough sodium and calcium enter the neuron, a threshold potential (-55 mV) is achieved, causing voltage-gated ion channels along the axon hillock to open.¹¹ The opening of these channels results in an influx of more sodium and calcium ions, fully depolarizing the cell and generating an action potential. This depolarization is at first localized but then diffuses down the axon, causing nearby voltage-gated channels to open, propagating the action potential.¹¹

Sodium channels are present at higher abundances and allow higher influxes of sodium to rush into the cell more rapidly, relative to calcium channels. The kinetics of voltage-gated calcium channel open/closure are slower than that of sodium.¹² Hence, sodium influx tends to drive rapid depolarization while calcium channels enhance depolarization and can also modulate neuronal excitability.¹² Different types of calcium channels open at different potentials, allowing them to modulate neuronal excitability outside of the context of a neurotransmitter binding event.⁹

As shown in figure 1.1, a single action potential in a healthy brain is characterized by a sharp but singular depolarization peak, followed by a refractory period in which the neuron hyperpolarizes before returning to its resting potential. In an epileptic brain, seizures occur when neurons synchronously exhibit high-frequency bursts of action potentials.⁵ As depicted in figure

1.1, during a seizure, multiple depolarization events happen in rapid succession without a return to the resting membrane potential.¹³ Moreover, the initial magnitude of the depolarization is much greater relative to typical single action potentials.¹³

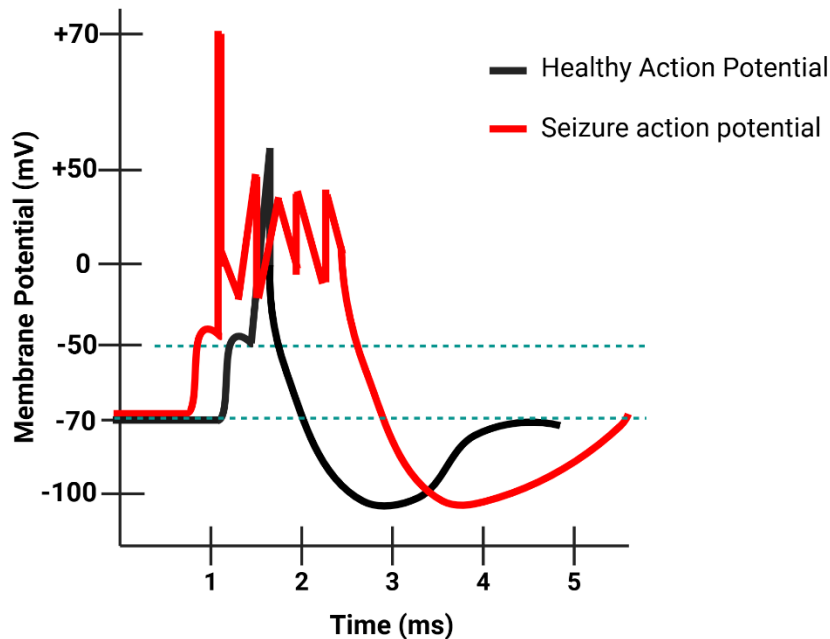


Figure 1.1: An action potential in a healthy brain overlaid with a rough depiction of an action potential that manifest during seizures in an epileptic brain. This figure is based on a figure in (Abbaszadeh et al, 2022).¹³

The development of hyperexcitable neurons can occur via various mechanisms. In many cases, increased calcium permeability raises the resting potential of the neuron, increasing the probability that stimuli will raise the membrane potential above the action potential threshold.^{14,15} Increased levels of excitatory neurotransmitters or decreased levels of inhibitory neurotransmitters may also increase the frequency of action potentials.⁵ An increase in the number of voltage-gated ion channels or decreases in the threshold potential can also play a role.¹⁶⁻¹⁸ Genetic epilepsies are frequently linked to alteration in the genes of ion channels.¹⁹ Changes in the cellular environment

may include alterations in ion concentration across the membrane, making the neuron more prone to depolarization.⁵

Cellular and Molecular Changes underlying Epileptogenesis

Epileptogenesis, the process by which a normal brain is converted to an epileptic brain with hyperexcitable neurons, can be summarized in a three-phase model.²⁰ The injury phase occurs when a precipitating event such as a trauma or a brain tumor progression initiates drastic changes in the cellular environment resulting in status epilepticus, a prolonged seizure lasting greater than 5 minutes.²⁰ After termination of the seizure, there is a latent phase where further alterations of pathways and cellular functions compound, leading to the development of spontaneous seizures.²⁰ Hence, the chronic phase is marked by the development of spontaneous recurrent seizures (SRS).^{20,21} Seizures beget seizures; each subsequent seizure contributes to the positive feedback loop of molecular changes, increasing the probability of further seizures. This three-phase progression is depicted below in Figure 1.2.

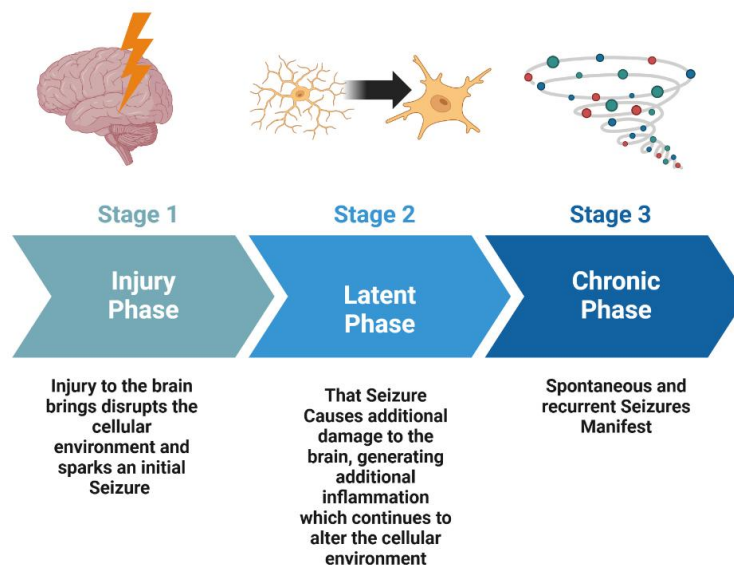


Figure 1.2: A three phase model that summarizes the transformation of a healthy brain into an epileptic brain (Created in <https://BioRender.com>).

A complete picture of the biochemical pathways underlying the three-phase development of epilepsy remains largely unresolved. Neuroinflammation is evident following seizures and is a complex response that involves many cells and molecules. However, the role of neuroinflammation as a cause and a consequence of seizures is still under investigation.^{22,23} This inflammation is promulgated mainly by immune cells in the nervous system, including resident microglia in the brain and circulating blood cells like monocytes.

Microglia are a subtype of glial cells. Glial cells, once thought to only play a structural role in the brain, perform a variety of tasks pertaining to metabolism, neuroprotection, and neurotransmission.²⁴ As the resident macrophages in the brain, microglia facilitate homeostatic maintenance by engulfing apoptotic cells and other cellular debris and releasing anti-inflammatory cytokines such as IL-10 in the process.²⁵ Under normal conditions microglia display a “resting phenotype” with a ramified shape and release low levels of inflammatory mediators. Rapidly following a seizure, microglia become activated, undergo morphology changes to adopt a proinflammatory phenotype, begin to proliferate, and release pro-inflammatory cytokines including but not limited to IL-6, TNF- α , CCL2, and IL-1 β in a process called microgliosis.²⁵⁻²⁷ Figure 1.3 depicts the morphology change of Microglia activated in-vitro.

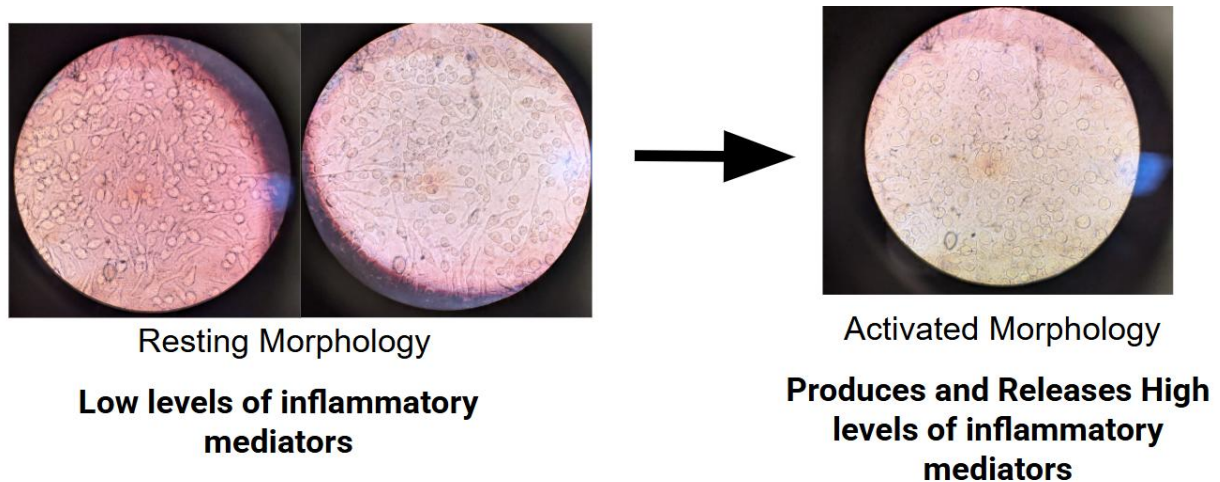


Figure 1.3: Morphology changes of Microglia under the microscope, following activation by Lipopolysaccharide (LPS).

Amongst the various elevated cytokines secreted by activated microglia, the increase in IL-1 β is sustained while elevated levels of TNF- α and IL-6 are transient.²³ Hence, it is suspected that IL-1 β elevation is a key cytokine that drives activation of downstream inflammatory pathways and initial seizure generation.

The release of cytokines and other inflammatory mediators, dominated by IL-1 β and Danger Associated Molecular Patterns (DAMPs) like HMGB1, drives the activation of Interleukin-1 receptor type 1 (IL-1R1) and toll-like receptor 4 (TLR4) in affected brain regions.^{22,28} These receptors are found on both resident microglia in the brain and circulating monocytes in the blood and are activated in response to the binding of cytokines and other endogenous danger-associated patterns (DAMPs), signals released by glial cells and neurons during pathological or stressed conditions.²⁹ Activation of IL_1R1 and TLR4 promotes neuronal hyperexcitability directly by triggering the phosphorylation of N-methyl-D-aspartate (NMDA) receptors.¹⁴ NMDA receptors are ligand-gated ion channels opened by glutamate binding. Phosphorylation of NMDA receptors increases their permeability to Ca²⁺ ions, leading to an influx of calcium into the

neuron.¹⁴ Upregulation of IL1-R1 and TLR4 also perpetuates an inflammatory cascade, summarized in figure 1.4, that induces the transcription of more pro-inflammatory genes including TNF- α , IL-6 cyclooxygenase-2 (Cox-2), nuclear factor kappa B (NFkB), and other cytokines.²⁸

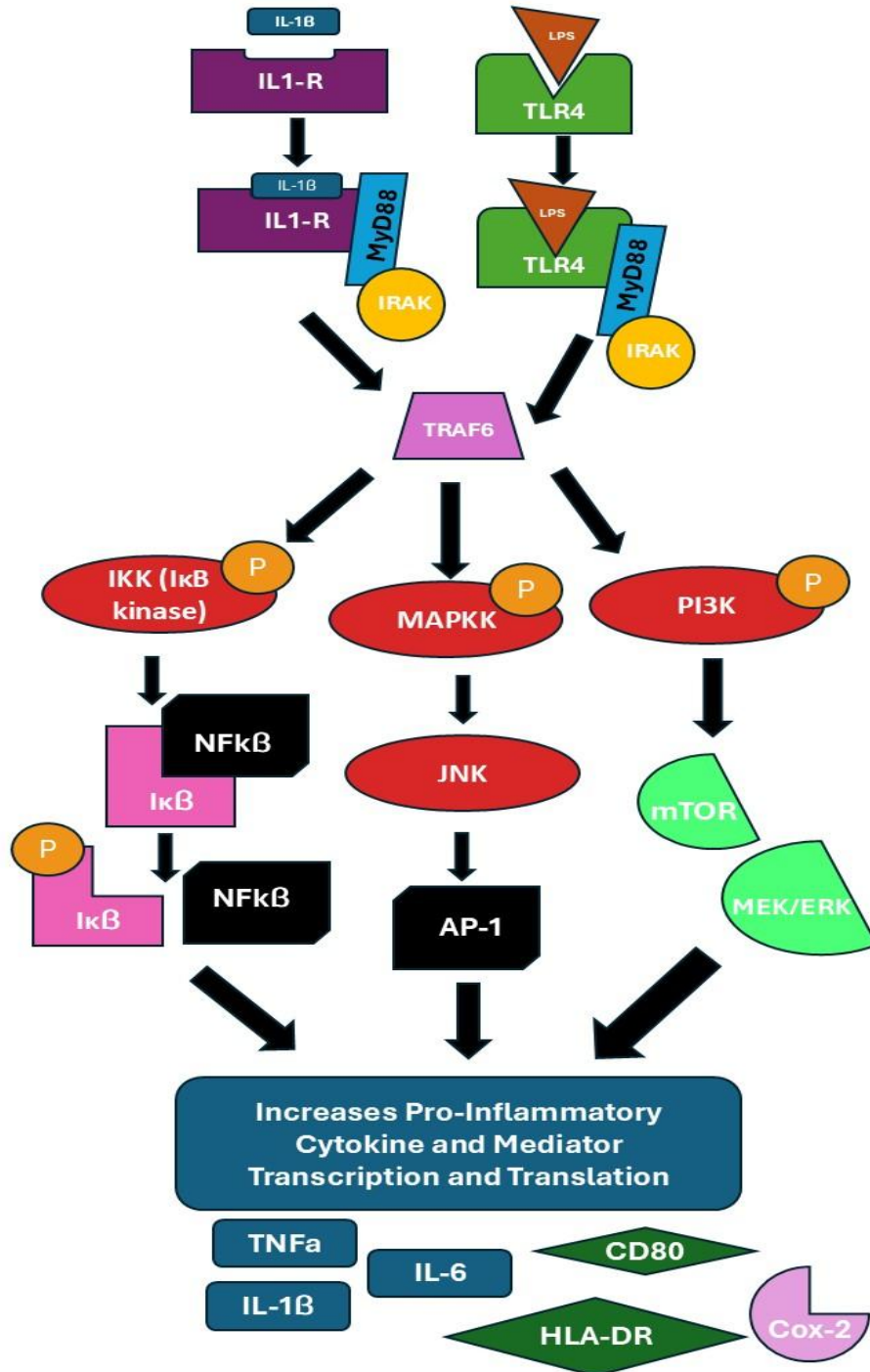


Figure 1.4: IL-1 β upregulation in Epileptogenesis increases activation of the depicted pathway, leading to the production of a variety of inflammatory mediators. Activation of this same pathway can be induced in-vitro in cells via LPS induction of the TLR4.

These pro-inflammatory cytokines not only perpetuate the positive feedback loop of the cytokine storm but also modify protein expression post-translationally to increase neuronal hyperexcitability. For example, elevated levels of TNF- α upregulate the expression of alpha-amino-3-hydroxy-5-methyl-4-isoxazolepropionic acid (AMPA) receptors that lack GluR2 subunits on the membrane.¹⁵ An AMPA receptor is another glutamate-controlled ligand-gated ion channel. The absence of GluR2 subunits makes AMPA more permeable to Ca²⁺ ions, increases single-channel conductance, and increases channel deactivation kinetics, resulting in larger but more short-lived excitatory postsynaptic potentials.¹⁵ TNF- α elevation also decreases the presentation of gamma-aminobutyric acid (GABA_A) receptors that bind inhibitory neurotransmitters, decreasing the frequency and strength of inhibitory synapses.²³ It has also been demonstrated that mice genetically modified to overexpress IL-6 have a lower seizure threshold.²³

In addition to generating inflammation and modulating the excitability of neurons, cytokines contribute to neurodegeneration via apoptotic and excitotoxic pathways. Inadequate clearance of excitatory neurotransmitters translates into repetitive burst of action potentials that, if persistent, culminate in neurodegeneration. Excitotoxic cell death occurs when too much glutamate or other excitatory neurotransmitters accumulate in the synaptic cleft.³⁰ This excess glutamate increases calcium influx which ultimately triggers proteases, phospholipases, and nucleases to break down the cell.³⁰⁻³² TNF- α increases glutamate release from both glial cells and neurons and also lowers the threshold potential for voltage-gated sodium channels.³³ IL-1 β , TNF- α , and IL-6 impair glutamate clearance by decreasing the expression of glutamate transporters on astrocytes.^{34,35}

There is also evidence that IL-1 β transiently increases blood-brain barrier (BBB) permeability via the disruption of tight junctions between endothelial cells, allowing molecules

that normally would not get into the brain entry into the brain.³⁶ This leakiness in the BBB allows the entry of innate and adaptive immune cells from the periphery to enter into the brain parenchyma.^{23,36} Elevated levels of CCL2, another pro-inflammatory cytokine secreted by the activated microglia, facilitate entry into the leaky BBB. The increased CCL2 gradient recruits blood-derived monocytes that express the receptor for CCL2 (CCR2).³⁶ Monocytes are derived from the same lineage as microglia.³⁷ Upon migration into the brain, monocytes adopt a macrophage-like phenotype that ranges on a spectrum between a “pro-inflammatory” phenotype (M1 Phenotype) and an “anti-inflammatory” phenotype (M2 Phenotype).³⁸ The exact fate of these monocytes and the pathways and conditions under which it is achieved are still uncertain. However, monocytes that resemble an M1 phenotype, behave similarly to activated pro-inflammatory microglia, releasing pro-inflammatory cytokines that modulate neuronal hyperexcitability and contribute to the positive feedback loop of inflammation.^{37,38} Previous work has demonstrated that CCR2 knockout mice display decreased levels of monocyte infiltration into the brain following status-epilepticus.³⁶ Importantly, in the absence of monocyte infiltration, opening of the BBB was decreased, suggesting that infiltrating monocytes work alongside microglia to perpetuate the inflammation that increases BBB permeability.³⁶ The decrease in monocyte infiltration also enhanced weight regain and decreased hippocampal neurodegeneration 3 days post-status epilepticus.³⁶ This indicates that monocytes significantly contribute to neuroinflammation associated with seizures.

The JAK/STAT pathway is a crucial mediator of cytokine-induced cellular changes

The mechanism by which cells respond to increased cytokines produced by monocytes and microglia relies on key downstream signaling pathways of the receptors such as the JAK/STAT pathway. The JAK/STAT pathway is one of the signaling mediators in cytokine expression and signal transduction in all cells.³⁹ Janus Kinases (JAK) are constitutively expressed multidomain non-receptor tyrosine kinases found on the cytoplasmic tails of select transmembrane cytokine receptors.⁴⁰ There are 4 known Janus Kinases: JAK1, JAK2, JAK3, and TYK2. Upon cytokines binding to their designated receptor, JAK becomes activated via dimerization and subsequent trans-autophosphorylation. Activated JAKs then phosphorylate and activate signal transducers and activators of transcription (STATs).³⁹ Upon phosphorylation, STATs dimerize, allowing them to be translocated into the nucleus where they act as a transcription factor, regulating gene transcription in pathways crucial for hematopoiesis, inflammation, cell growth/survival, development, and stem-cell maintenance, just to name a few.³⁹⁻⁴¹

Unlike the other members of the JAK family, which are ubiquitously expressed and whose deletion results in “perinatal and embryonic lethality”, JAK3 is primarily expressed in lymphoid cells and only directly regulates transduction on cytokine receptors that possess the common gamma chain subunit.^{42,43} The deletion of JAK3 is non-lethal; JAK3 knockout mice remain viable while displaying a severe immunodeficiency phenotype.⁴² Consequently, in diseases where inflammation is persistent and abnormally elevated, JAK3 is an attractive and pharmacological target due to its specificity.

There is some debate as to whether JAK3 inhibition on its own is effective in the treatment of autoimmune diseases and other conditions in which an excessive inflammatory response is observed.⁴⁴ Historically, without the crystal structure of JAKs, and due to their structural

homology, it was difficult to develop an inhibitor with exclusive specificity towards JAK3. As insights into JAK structures advance, some still seek to develop inhibitors that dually act on JAK3 and JAK1.⁴⁴ It is thought that optimal treatment of autoimmune diseases requires some targeting of JAK1 due to its presence on many of the common γ c-containing cytokine receptors, often in conjunction with JAK3.⁴⁴ In fact, without JAK1 inhibition, JAK3 inhibition alone only partially blocks cytokine signaling.⁴⁵

JAK Structure and Chemistry

The structure of all JAKs was initially divided into 7 JAK Homology Domains (JH1-JH7), based on sequence homology.³⁹ However, the elucidation of the crystal structure of JAKs reveals four functional domains.³⁹ JAKs (Janus Kinases) derive their name from the two-faced Roman God because they are single polypeptide chains consisting of two kinase domains. JH1, the tyrosine kinase domain that is mostly conserved amongst all JAKs, starts at the carboxylic acid terminal, constituting the first 275 amino acids of the primary sequence, and serves as the catalytic domain.⁴⁶

The kinase domain is constituted of a small N-terminal lobe connected to a large C-terminal lobe by a short kinase hinge.^{47,48} These lobes form a binding cavity in which an incoming ATP substrate is sandwiched between the N-terminal lobe above and the C-terminal lobe below, abutting the kinase hinge.^{47,48}

The N-terminal lobe is composed of a 5-stranded beta-sheet and singular alpha helix while the C-terminal lobe is primarily composed of alpha helices.^{47,48} In the N-terminal lobe, between the first and second beta strands, resides a glycine-rich ATP-phosphate-binding loop. This binding loop contains a GxGxΦG motif which engages in hydrogen bonding with anchoring ATP and

stabilizing its binding to the kinase.^{47,48} The third beta-strand contains a lysine which engages in salt-bridge interactions with the alpha and beta phosphate groups on ATP.^{47,48}

The kinase hinge, the loop motif that links the N-terminal and C-terminal lobe, also interacts with ATP via hydrogen bonding. As shown below in Figure 1.5, two nitrogen on ATP form two hydrogen bonds with the backbone of two residues on the kinase hinge to secure it to the binding cleft. The nitrogen at the 6th position of ATP's adenine ring hydrogen bonds to the carbonyl on the backbone of the first residue of the kinase hinge and the nitrogen on the 1st position of the adenine ring hydrogen bonds to the backbone of the 3rd residue.⁴⁸



Inside the JH1 Domain:

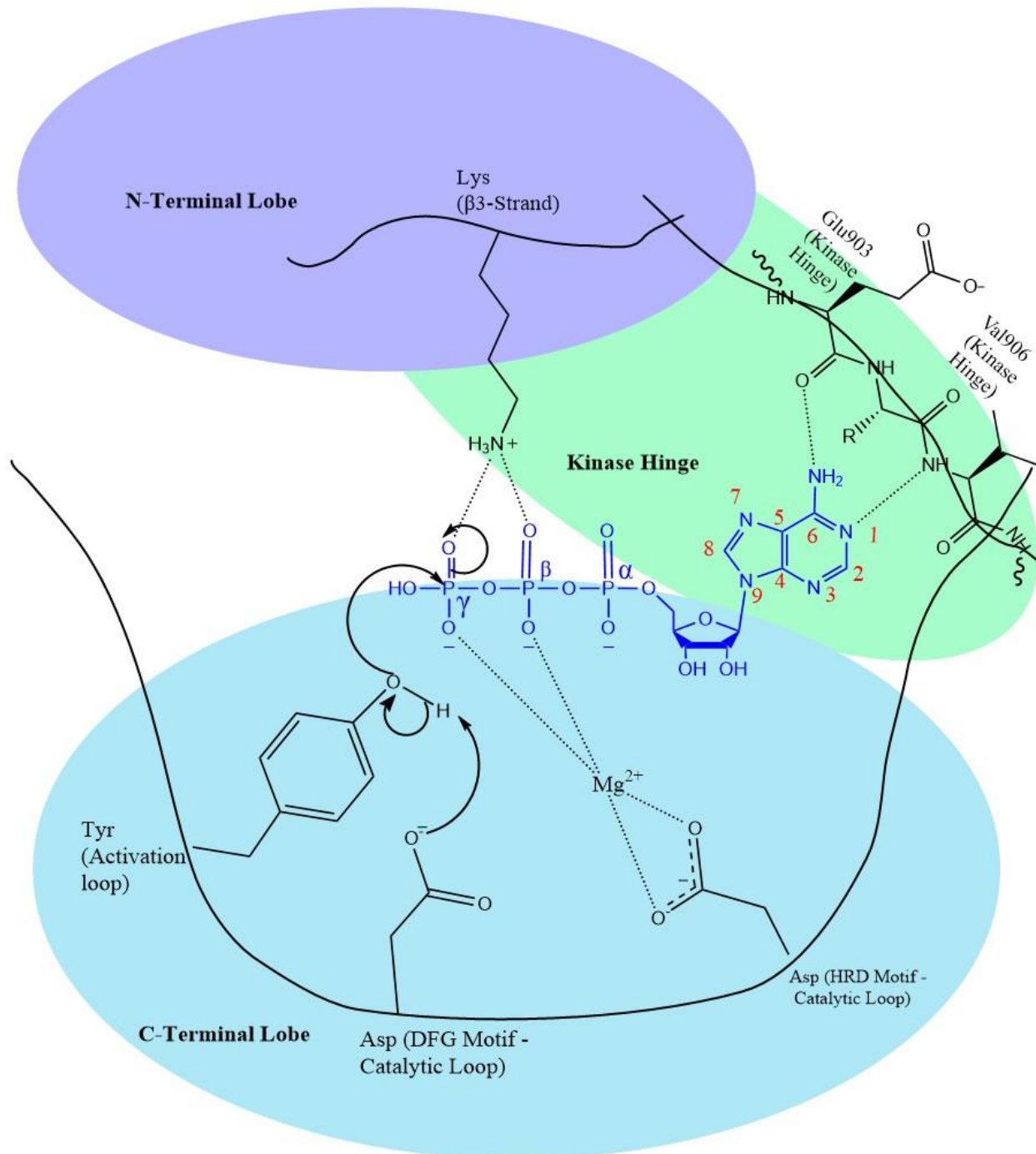


Figure 1.5: An illustration depicting key residues in the binding pocket on JH1

Steady-state competitive JAK inhibitors, like Tofacitinib, mimic the structure of ATP while optimizing hydrogen bond interactions with the kinase hinge to block ATP from accessing the binding cleft.⁴⁸ JAK1, JAK2, JAK3, and TYK2 have slightly different residues at the 1st and third position, allowing for inhibitor specificity.⁴⁸ Of note, JAK1 and JAK3 are the only two JAKs that both have a glutamate and a leucine as the 1st and 3rd residues on the kinase hinge, respectively.⁴⁸

The c-terminal lobe contains a catalytic loop and an activation loop. One of two adjacent tyrosine residues on the activation loop engages in a nucleophilic attack on the γ -phosphate of ATP.^{47,48} This nucleophilic attack is facilitated by a histidine-arginine-aspartate motif (H-R-D motif) and an Aspartate-Phenylalanine-Glycine motif (D-F-G motif) on the catalytic loop.^{47,48} The Aspartate on the H-R-D Motif acts as a general base, increasing the nucleophilicity of tyrosine by deprotonating it. The Aspartate on the D-F-G motif chelates Mg^{2+} . A divalent cation, like Mg^{2+} , coordinates with ATP's α - β - and γ -phosphates and is crucial for establishing the correct orientation for phospho-transfer.^{47,48} The chemical reaction facilitated by the kinase domain is depicted above in Figure 1.1. There are several other residues on the kinase domain that stabilize the binding of ATP to JAK. This includes another asparagine on the activation loop that contributes to Mg^{2+} chelation.⁴⁸

Another set of hydrophobic residues that exist on both the c-terminal lobe and n-terminal lobe constitute the hydrophobic catalytic (C-Spine) and regulatory (R-spine) spines that assemble upon ATP binding.^{49,50} These hydrophobic spines in the catalytic core stabilize the bound ATP and influence its orientation for catalysis. The C-Spine consists of hydrophobic residues on the N-terminal lobe and C-terminal lobe, linked by the adenine ring. The R spine runs parallel to the C-Spine, engaging two aromatic residues from the C-lobe, including the phenylalanine from the DFG

motif, and two aliphatic residues from the alpha-helix and β_4 strand on the N-lobe.^{49,51} Again, the positions of these residues and motifs differ slightly between the different JAKs, allowing for specificity to be built into any potential inhibitor.

The pseudokinase domain contains a similar structure and sequence to the kinase domain with differences in key residues that render it largely catalytically inactive. For instance, the aspartate on the H-R-D motif on the catalytic loop is replaced by an asparagine, which is incapable of deprotonating tyrosine.⁴⁸ In the D-F-G Motif, proline replaces phenylalanine, creating a conformation in which the chelating aspartate lies deeper in the binding cleft and becomes hard to access.⁵² The pseudokinase domain also lacks the third glycine in a GXGXXG motif on the n-terminal lobe which is crucial for orienting and anchoring ATP.⁵³

The N-terminal lobe of the pseudokinase domain interfaces with the N-terminal lobe of the kinase domain at a 90° angle, facilitated primarily by hydrophobic interactions between a phenylalanine residue on the pseudokinase domain and hydrophobic residues on the kinase domain (Ile, Leu, Met, and Tyr).⁵² Pseudokinase regulates the kinase domain in an autoinhibitory manner as shown by the higher K_m and lower activity associated with ATP binding to the pseudokinase–kinase protein complex relative to ATP binding to the Kinase domain in isolation.⁵² The SH₂ and FERM domains primarily mediate the interaction of JAK with the receptor tails.⁵⁴

Prior to cytokine binding to their respective receptors, the tyrosine kinase is held in a closed or inactive conformation via stabilizing intramolecular interactions with the pseudokinase.⁴⁶ In this inactive state, not only is kinase mobility restricted but it is thought that the JH1-JH2 interaction facilitates a DFG flip, where the order of aspartate and phenylalanine residues temporarily switch positions, leading to a “DFG-out” conformation where the Mg²⁺-chelating aspartate is pointed away from the active site.⁵⁵ Other modeling studies have proposed that, in the inactive state, the

tyrosine kinase “is folded back on the FERM-SH2 domain” which not only blocks ATP from accessing the binding pocket but generates steric repulsion between the FERM and pseudokinase domains between JAKs that would otherwise dimerize.⁵⁶

Upon cytokine binding, a conformation change is induced in which the pseudokinase domain and kinase domain become separated via a rotation.^{48,57} This separation allows the JAK on one receptor to dimerize with another JAK on a proximal receptor, thereby facilitating the trans-autophosphorylation of the JAKs.⁵⁷

Once JAKs are activated, they phosphorylate tyrosine residues located on the intracellular cytoplasmic domain. The exact mechanism and conformation changes required for this phosphorylation are not yet fully understood.⁵⁶ Nonetheless, this creates docking sites for STATs which attract and bind to the SH₂ domain of two STAT proteins via interactions between the phosphate group and conserved residues on the SH₂ domain.⁴⁶ Upon docking, JAK phosphorylates a tyrosine residue on the transcriptional activation domain of the bound STAT.^{39,48} The resulting phosphotyrosine on one STAT protein binds to the SH₂ domain on a neighboring phosphorylated tyrosine and vice-versa, creating a pSTAT dimer in an antiparallel β -strands arrangement.⁴⁶ Dimerization displaces the SH₂ domain interactions with the receptor, causing the pSTAT dimer to dissociate from the receptor and translocate from the cytoplasm into the nucleus where its DNA binding domain binds to target sequences and either suppresses or enhances transcription.⁴⁶ Shown below in Figure 1.6, is a schematic of the pathway.

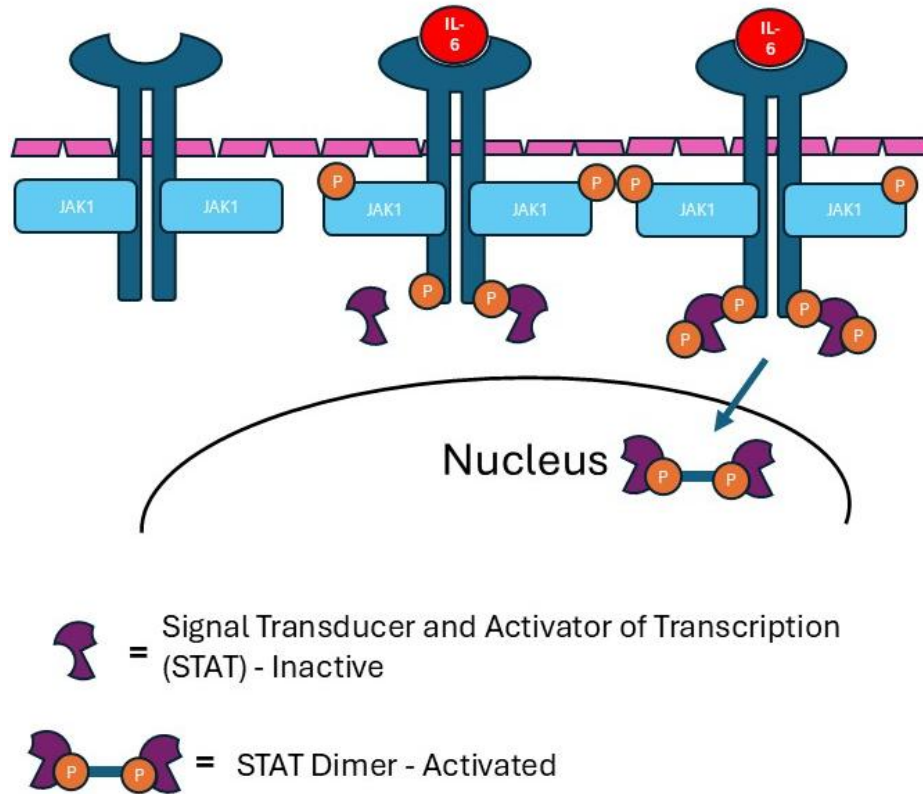


Figure 1.6: A depiction of the JAK/STAT phosphorylation mechanism.

There are 7 STATs that homodimerize and heterodimerize in a variety of combinations to induce the transcription of different proteins. For instance, STAT1 activation initiates the transcription of apoptosis proteins such as caspase 1.⁴⁶ STAT1 has also been implicated in inducing M1 macrophage polarization downstream of TLR signaling.⁵⁸ Conversely, STAT3/STAT6 dimers promote M2 macrophage polarization.⁵⁸

Tofacitinib (CP-690,550) Mechanism of Inhibition

Tofacitinib (CP-690,550), is a small molecule PAN-JAK competitive inhibitor, initially developed by Pfizer to treat autoimmune diseases such as Graft vs Host Disease and Rheumatoid Arthritis.⁵⁹ CP-690,550 is highly potent against JAK3 with a K_i of 0.2 nM. It inhibits JAK1 ($K_i=0.7$ nM), JAK2 ($K_i=1$ nM), and TYK2 ($K_i=4.4$ nM) with lower potency.⁶⁰ Its high specificity towards

the JAK kinases within the human kinome is remarkable, considering that, at the time of its development, the structure of JAK was unknown.⁵⁹ The structure of CP-690,550 is shown below in Figure 1.7.

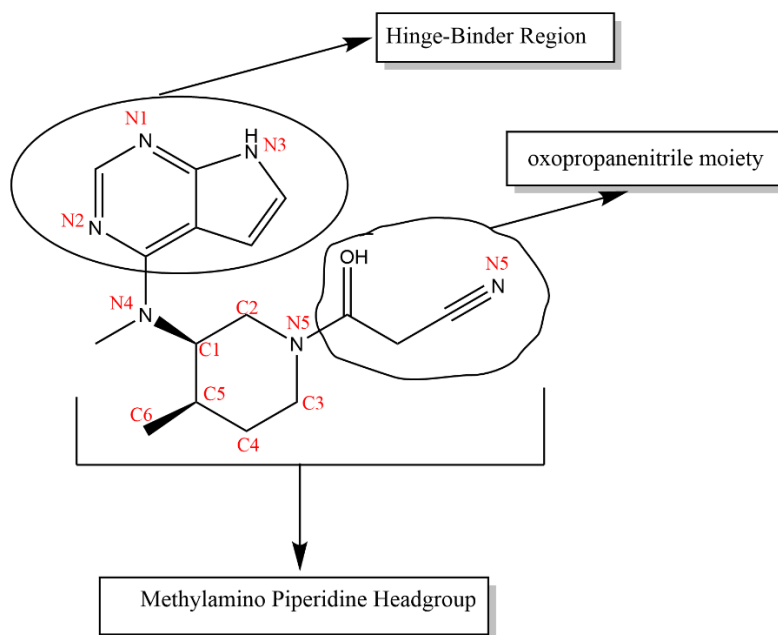


Figure 1.7: The Chemical structure of CP-690.550

CP-690,550 consists of a pyrrolopyrimidine hinge binder group that bears a high structural resemblance to Adenine in ATP. The hinge binder group is attached to a methylamino piperidine headgroup with an oxopropanenitrile moiety bonded to the nitrogen on the piperidine ring.⁵⁹ The pyrrolopyrimidine ring is oriented against the kinase hinge.⁶⁰ Analogous to ATP, it creates two hydrogen bonds with the 1st and 3rd residues of the kinase hinge; In JAK3, the N-H on the polypyrrole forms a hydrogen bond with the carbonyl on the 1st glutamate residue, and the nitrogen on the 1st position of the adenine ring hydrogen bonds to the N-H of the backbone of the 3rd residue, leucine. The piperidine headgroup is oriented to allow it to engage in hydrophobic

interactions. Specifically, the C6 methyl group points towards the C-lobe while the cyano group on the other side of the ring forms polar contacts glycine-rich loop, obstructing another key anchoring point of ATP.^{48,60} This is in addition to the many interactions CP-690,550 engages in with the aforementioned hydrophobic spines. Tofacitinib's high selectivity of JAK3 is attributed to the manner in which it binds. Tofacitinib binds the "DFG-in" active conformation of the kinase.⁶¹ However, specifically with JAK3, it favorably binds in such manner that it causes the kinase to adopt of peculiar closed conformation in which an asparagine residue on the N-terminal lobe engages in hydrogen bonding with the carboxy group on ASP949, the catalytic aspartate.⁶¹ This structure causes the N-lobe to be twisted against the C-lobe.⁶¹ Hence, Tofacitinib does not just block ATP's access to the hinge binding region but, effectively, the whole catalytic subunit.

Administration of Tofacitinib to Epileptic Mice Decrease Seizure Severity and Frequency

Recently, single nucleus RNA sequencing (RNAseq) analysis performed on hippocampal tissue from pilocarpine-treated mice that was harvested 4 days after status epilepticus revealed that "STAT3 was among the top three genes controlling upregulated gene expression across the greatest number of cell types".² This finding was replicated in transcriptome data from human temporal lobectomy samples from patients with chronic epilepsy. The same study found that the JAK/STAT pathway is active immediately following status epilepticus in both neurons and glial cells but subsides in activity in the days following.² Upon the recurrence of a spontaneous seizure, the JAK/STAT pathway once again demonstrates an uptick in activity.² The study further demonstrated that daily administration of CP-690,550 to chronically epileptic mice reduced both seizure frequency by 80% along with seizure severity.² When CP-690,550 was withdrawn from the 65% of mice that responded to the treatment, 75% of those mice remained seizure-free.² Not

only did CP-690,550 suppress seizures but it also demonstrated the ability to reverse cognitive comorbidities associated with chronic seizures.²

It remains to be known which pathways downstream of JAK/STAT activation are being inhibited by CP-690,550 and in which cell population to produce the reduction in seizure severity and frequency. One possibility is that the reduction in seizure severity and frequency is due to a direct suppression of inflammatory cytokine expression and release by monocytes and microglia, and not just a disruption in transduction. Therefore, the hypothesis is, by directly inhibiting the JAK/STAT pathway, CP-690,550 reduces the production of inflammatory mediators by microglia and monocytes.

To test this hypothesis, we developed and optimized an in-vitro inflammatory model, using lipopolysaccharide (LPS) to stimulate THP1 monocytes and BV2-hEP2 microglia in culture. LPS causes inflammation by binding to and directly activating TLR4 which is believed to be activated very early on following seizures. After establishing the optimal working LPS dose to induce M1 macrophage polarization and using TAK-242 to confirm that M1 macrophage polarization is contingent on LPS activation of TLR4, we exposed monocytes and microglia to various doses of Tofacitinib and investigated the effect on multiple LPS-induced pro-inflammatory mediators including IL-1 β , TNF- α , IL-6 and Cox-2 at both the mRNA level measured by qRT-PCR and the protein level by western blot. We also investigated the impact of Tofacitinib's effectiveness at modulating post-translational modification of downstream targets.

2. Material and Methods

2.1 BV2-hEP2 Microglia Cell Line

The BV2 microglia were generously provided by Dr. Malu Tansey (Emory University, Atlanta, GA). BV2 cells were stably transfected with human EP2 as previously described (Rojas et al., 2019).⁶² Briefly, murine-derived BV2 microglia were transfected with human EP2 (Accession no. AY275471) in the pcDNA3.1(+) vector (University of Missouri-Rolla cDNA resource center) using Lipofectamine 2000 transfection reagent (Invitrogen) according to the manufacturer's protocol. Following transfection, the cells were allowed to grow and proliferate for 48 hours prior to incubation in complete media supplemented with 400 µg/mL G418 (Sigma-Aldrich, St. Louis, MO). After a week of incubation in the presence of G418 the culture was subcloned by limiting dilution. BV2-hEP2 subclones were expanded from a single cell and maintained in complete medium supplemented with 800 µg/mL G418 (Sigma-Aldrich) at 37 °C in 95% air/5% CO₂. BV2-hEP2 cells were cultured in Dulbecco's Modified Eagle Medium Nutrient Mixture F-12 containing L-Glutamine and Sodium bicarbonate. The medium was supplemented with 10% Fetal Bovine Serum (FBS), as a source of growth factors and proteins, and 10% Penicillin-streptomycin to prevent bacterial contamination. Cells were maintained in a T-75 flask and passaged every 4 days. To passage the cells, the media was removed from the flask and discarded. The cells attached to the bottom of the flask was washed twice with PBS and then incubated with 0.25% Trypsin-EDTA for 5 minutes at 37 °C to detach the cells. Media was then added to the flask to deactivate the trypsin and the cells were collected, counted and either transferred to a new flask or plated in plates for subsequent experiments.

2.2 THP1 Monocyte Cell Line

The THP1 monocyte cell line, derived from a human leukemia patient and named for Tohoku Hospital Patient (THP), was cultured in sterile-filtered RPMI-1640 High Glucose Media with L-Glutamine and HEPES, a buffering agent. The media was further supplemented with 10% FBS, 10% Penicillin-streptomycin, and an additional 10% HEPES. The media was also supplemented with 10% sodium pyruvate, imperative for facilitating ATP production in a high glucose environment. Cells were maintained in a T-75 flask at 37 °C in 95% air/5% CO₂ in suspension and passaged every 5 days by pelleting and reseeding the cells in fresh media.

2.3 THP1 Monocyte LPS Optimization and Cell Dosing (protein extraction)

THP1 cells were plated in a sterile 6-well plate at a confluency of 1,000,000 cells per well and allowed to acclimate and adhere to the plate for 24 hours. Each well was treated with lipopolysaccharide (LPS) dissolved in water at various concentrations (0 ng/mL, 0.1 ng/mL, 1 ng/mL, 10 ng/mL, 100 ng/mL of LPS). The LPS stock was dissolved to maintain the same concentration of DMSO which was lower than 1% for all concentrations used. Treated cells were then incubated for 24 hours before being collected and pelleted at 2,000 RPM for 5 minutes. The cells were collected in a tube and pelleted by centrifugation to extract total protein. The cell pellet was resuspended in RIPA lysis and extraction buffer (Supplemented with 100x Phosphatase Inhibitor and 100x Protease Inhibitor). The lysate was incubated on a platform rocker for 20 minutes at 4 ° Celsius and sonicated to further lyse the cells and solubilize the protein. The cell lysates were centrifuged to separate any cellular debris left after the extraction process. The total protein from the soluble fraction in each lysate was quantified and further prepared for western blot described below in section 2.7.

2.4 THP1 Monocyte and LPS/TAK-242 Cell Dosing (protein extraction)

THP1 cells were plated in a 6-well plate at a confluency of 1,000,000 cells per well and allowed to acclimate and adhere to the plate for 24 hours at 37°C. Cells were then treated with 10 µM TAK-242 (dissolved in DMSO), a toll-like receptor 4 (TLR4) inhibitor, or DMSO only in 1x Phosphate Buffered Saline (PBS) for 1 hour. Thereafter cells were treated with 10 ng/mL of LPS or water which was used as the vehicle for LPS. Treatment groups included DMSO, DMSO/TAK-242, DMSO/LPS, and LPS/TAK-242. Treated cells were then incubated for 24 hours before being collected and pelleted at 2000 RPM for 5 minutes. Total protein was extracted, separated into soluble and insoluble fractions, quantified, and prepared for western blot experiments as described above in section 2.3.

2.5 Working Tofacitinib Stock Solution:

CP-690,550 citrate (C₁₆H₂₀N₆O), also known as Tofacitinib Citrate, was provided by Tocris and dissolved in DMSO to make a 0.935 µM working solution. This working solution was further serially diluted in DMSO to obtain lower concentrations of the drug for subsequent experiments.

2.6 Western Blot:

Protein lysates were quantified via a Bicinchoninic Acid (BCA) protein assay. The assay relies on the interaction of peptides with Copper (II) Sulfate. The peptides reduce the Cu²⁺ to Cu⁺ which, at high temperatures, forms a colored purple complex whose absorption at 562 nM varies proportionally with protein concentration. The protein samples are quantified against a standard curve. Once the protein was quantified, samples were mixed with 4x Laemli buffer containing loading dye and beta-mercaptoethanol as a reducing agent to linearize proteins and then heated at 70 ° C for 7 minutes. Total protein lysates (20 µg of total protein) were separated by size using a

4-20% gradient sodium dodecyl sulfate polyacrylamide gel by electrophoresis (SDS-PAGE) for 1 hour at 150 mV and electroblotted onto polyvinylidene fluoride (PVDF) membranes (88520, Millipore, Burlington, MA) for 16 hours at 30 mV. Membranes were blocked with 5% (w/v) non-fat milk at 25 °C for 1 hour and subsequently incubated overnight at 4 °C with the primary antibody: rabbit anti-IL-6 (1:1000, 12153S Cell Signaling Technology, Danvers, MA), mouse anti-IL-1 β (1:1000, 12242S, Cell Signaling Technology, Danvers, MA), rabbit anti-STAT (1:1000, 30835T, Cell Signaling Technology) or mouse anti-pSTAT (1:1000, 4113T, Cell Signaling Technology). Glyceraldehyde 3-phosphate dehydrogenase (GAPDH) (1:1000, ab181602, Millipore) and heat shock protein 60 (HSP60, 1:1000, ab5622, Millipore) were used as internal loading controls. The blots were washed three times for 5 minutes each with tris buffered saline containing tween-20 (TBST). After washing, the blots were incubated with goat anti-rabbit (111-035-003) or goat anti-mouse (115-035-003) horseradish peroxidase-conjugated secondary antibodies (1:2000, Jackson Immuno, West Grove, PA) at room temperature for 1 h. The blots were washed again (3x, 5 min each), developed by enhanced chemiluminescence (Immobilon Western Chemiluminescent HRP Substrate) (Millipore Sigma, Burlington, MA), and scanned using a ChemiDoc MP imaging system (12003154, BioRad, Hercules, CA). The band intensities were quantified directly from the .scn file by ImageLab 6.0.1 (BioRad). For each sample, the protein quantification was normalized to the loading control and expressed as the fold change relative to the corresponding control samples.

2.7 RNA isolation and quantitative real-time polymerase chain reaction (qRT-PCR)

Total RNA was extracted using the Zymo Research Quick-RNA Microprep kit reagents and protocol. The RNA concentration and purity were measured by a SmartSpec 3000 spectrophotometer (Biorad, Hercules, CA) using the A260 value and the A260/A280 ratio,

respectively. RNA was converted into cDNA by adding 1 μg of RNA to a 20 μL reaction mix with 4 μl of Quantabio qScript cDNA Supermix (contains M-MLV reverse transcriptase, ribonuclease inhibitor protein, Deoxynucleotide triphosphates (dNTPs), primers, and enzyme stabilizers). The First-strand cDNA synthesis reaction was performed at 42 $^{\circ}\text{C}$ for 50 min. The reaction was terminated by heating at 70 $^{\circ}\text{C}$ for 15 min. RNA from the THP1 cells (1 μg total RNA) and the BV2-hEP2 cells (2 μg total RNA) was converted to cDNA.

The newly synthesized cDNA was diluted and then added to qRT-PCR reaction mixes on a 96-well plate, containing 8 μl of 10x diluted template cDNA, SYBR green, HotStart DNA Taq polymerase, dNTPs, Taq buffer, and forward and reverse primers at a total concentration of 1 μM (0.5 μM forward primer, 0.5 μM reverse primer) with a final volume of 20 μl . qRT-PCR reactions were run in the iQ5 Multicolor Real-Time PCR Detection System (Bio-Rad). Cycling conditions were as follows: 95 $^{\circ}\text{C}$ for 2 min followed by 40 cycles of 95 $^{\circ}\text{C}$ for 15 sec and 60 $^{\circ}\text{C}$ for 1 min. Melting curve analysis was used to verify the specificity of the primers by single-species PCR product. Fluorescent data were acquired at the 60 $^{\circ}\text{C}$ step. Samples without cDNA template served as the no-template controls. The threshold cycle (Ct) values for each gene in each treatment group were obtained at the end of each PCR. The mean of cycle thresholds for mouse β -actin and glyceraldehyde-3-phosphate (GAPDH) was used as an internal control for relative quantification. Cycle threshold (Ct) values for each gene in each treatment group were obtained and converted into fold-change values, after standardizing them to the Average Ct values of the housekeeping genes (actin and GAPDH). Analysis of quantitative real-time PCR data was performed by subtracting the average mean of two internal control genes from the measured cycle threshold value obtained from the log phase of each amplification curve of each gene of interest. The fold increase of each gene of interest was estimated for each treatment relative to the amount

of RNA found in the control samples using the $2^{\Delta\Delta CT}$ method.⁶³ The sequences for the primers of the targeted genes of interest (mouse and human) are listed below in Table 2.1 and Table 2.2.

Table 2.1: Mouse Primer Sequences

Gene	Forward Primer Sequence	Reverse Primer Sequence
β -Actin	5'- AAG GCC AAC CGT GAA AAG AT -3'	5'- GTG GTA CGA CCA GAG GCA TAC -3'
GAPDH	5'- TGT CCG TCG TGG ATC TGA C -3'	5'- CCT GCT TCA CCA CCT TCT TG -3'
Cox-2	5'- CTC CAC CGC CAC CAC TAC -3'	5'- TGG ATT GGA ACA GCA AGG AT -3'
IL-1 β	5'- TGA GCA CCT TCT TTT CCT TCA -3'	5'- TTG TCT AAT GGG AAC GTC ACA C-3'
TNF- α	5'- GGT GCC TAT GTC TCA GCC TCT T -3'	5'- GCC ATA GAA CTG ATG AGA GGG AG -3'
IL-6	5'- TAC CAC TTC ACA AGT CGG AGG C -3'	5'- CTG CAA GTG CAT CAT CGT TGT TC -3

Table 2.2: Human Primer Sequences

Gene	Forward Primer Sequence	Reverse Primer Sequence
B-Actin	5'- CAC CAT TGG CAA TGA GCG GTT C-3'	5'- AGG TCT TTG CGG ATG TCC ACG T -3'
GAPDH	5'- TGT CCG TCG TGG ATC TGA C -3'	5'- CCT GCT TCA CCA CCT TCT TG -3'
Cox-2	5'- CGG TGA AAC TCT GGC TAG ACA G -3'	5'- GCA AAC CGT AGA TGC TCA GGG A -3'
CCR2	5'- TGG CTG TGT TTG CTT CTG TC -3'	5'- TCT CAC TGC CCT ATG CCT CT -3'
CD80	5'- CTC TTG GTG CTG GCT GGT CTT T -3'	5'- GCC AGT AGA TGC GAG TTT GTG C-3'
IL-6	5'- AGA CAG CCA CTC ACC TCT TCA G -3'	5'-TTC TGC CAG TGC CTC TTT GCT G -3'

2.8 THP1 Monocyte and Tofacitinib/LPS Dosing (RNA isolation)

THP1 monocytes were plated in a 12-well plate at a confluency of 400,000 cells per well and allowed to acclimate for 24 hours. Thereafter, the plate was separated into treatment groups consisting of two replicates and treated with either DMSO, 1 nM, 10 nM, 100 nM, or 1000 nM of Tofacitinib. After an incubation period of two hours with the Tofacitinib at 37°C, the cells were treated with 10 ng/mL of LPS for an additional two hours. One group treated with DMSO only and not LPS was used to establish a baseline for inflammatory cytokine expression. Following treatment with LPS, the cells were collected and centrifuged at 500 xg for 5 minutes. The pellets were then resuspended in RNA lysis buffer. Samples were then processed for qRT-PCR as described above.

2.9 BV2-hEP2 Cells and Tofacitinib/LPS Dosing (RNA isolation)

BV2-hEP2 cells were plated in a 12-well plate at a confluency of 400,000 cells per well and allowed to acclimate and adhere to the plate for 24 hours. Thereafter, the plate was separated into treatment groups consisting of two replicates and treated with either DMSO, 1 nM, 10 nM, 100 nM, or 1000 nM of Tofacitinib. DMSO can inhibit cytokine production, hence to isolate the effects of Tofacitinib, DMSO serves as the control group.⁶⁴ DMSO was maintained at a concentration of less than 1% in all treatments. After a 2-hour incubation period with the drug, the cells were treated with 10 ng/mL LPS for an additional two hours. One group did not receive LPS but were exposed to DMSO to establish a baseline for inflammatory cytokine expression. Following treatment with LPS, the cells were washed with cold 1x PBS to suspend metabolic and enzymatic activity and lysed with RNA lysis buffer before being collected and pelleted. Samples were lysed and then processed for qRT-PCR analysis as described in detail

below. The only deviation from the described qRT-PCR protocol is that 2 µg of RNA were converted to cDNA instead of the standard protocol of using 1 µg of RNA.

2.10 BV2-hEP2 Cells qRT-PCR and Primer Validation

BV2-hEP2 cells were plated in a 12-well plate at a confluency of 400,000 cells per well and allowed to acclimate and adhere to the plate for 24 hours. Cells were treated with 10 ng/mL LPS for two hours at 37 degrees Celsius. Following treatment with LPS, the cells were washed with cold PBS to suspend metabolic and enzymatic activity and lysed with RNA lysis buffer before being collected from the plate. Samples were then processed for qRT-PCR analysis as described above. Transcribed cDNA was serially diluted in water at the following concentrations: 10x, 100x, 1000x, 10,000x. qRT-PCR was performed for all primers used in prior BV2-hEP2 experiments as described above.

2.11 BV2-hEP2 Cells Tofacitinib/LPS Dosing to Observe Tofacitinib's Effect on Post-Translation Modifications (protein isolation)

BV2-hEP2 cells were plated in a 6-well plate at a confluency of 1,000,000 cells per well and allowed to acclimate and adhere to the plate for 24 hours. Each well was treated with either DMSO, 1 nM of Tofacitinib, 10 nM of Tofacitinib, 100 nM of Tofacitinib, or 1000 nM of Tofacitinib for two hours. After incubation with the drug, cells were treated with 10 ng/mL of LPS and allowed to incubate at 37°C for 24 hours. One of the two DMSO treatment groups did not receive LPS to establish a baseline for inflammatory cytokine expression. Following treatment with LPS, the cells were washed with cold PBS to suspend metabolic and enzymatic activity. Treated cells were then incubated for 24 hours before being collected and pelleted at 2000 RPM for 5 minutes. Total protein was extracted, separated into soluble and insoluble fractions, quantified, and prepared for western blot experiments as described above in section 2.3.

2.12 Data analysis and statistics

Concentration–response curves were made using GraphPad Prism software (Version 8). Statistical analysis was performed using GraphPad Prism software with one-way ANOVA and post hoc Bonferroni with selected pairs. For the cytokine induction assays, $\Delta\Delta\text{CT}$ values were used for statistical analysis while fold changes are represented in the graphs. Differences were considered to be statistically significant if $p < 0.05$. All data are presented as mean \pm SEM.

3. Results

3.1 LPS Induction as a Model for Neuroinflammation in THP1 Cells

Lipopolysaccharide (LPS) is a glycolipid that resides on the outer membrane of gram-negative bacteria. LPS contains the hydrophobic lipid A moiety whose acyl tails specifically bind to the hydrophobic pocket of the MD-2 receptor.⁶⁵ The phosphate groups above the acyl tails engage in hydrogen bonding and ionic interactions with residues on the MD-2 receptor. MD-2 then complexes with and activates TLR4, initiating an inflammatory cascade.⁶⁵ LPS activation of TLR4 leads to an increase of pro-inflammatory cytokines along the same pathway activated by IL1-B/DAMP, that is thought to drive inflammation the beginning of epileptogenesis.⁶⁵ A depiction of this pathway is shown above in Figure 1.4. Thus, LPS can be used as an in-vitro agonist to evaluate the effects of CP-690,550 on inflammation in cells cultured in a controlled environment.

To determine the optimal dose of LPS to polarize THP1 monocytes into a pro-inflammatory M1 phenotype, a dose response was tested to examine the impacts of different concentrations of LPS on the protein expression levels of pro-inflammatory cytokines, IL-6 and human leukocyte antigen HLA-DR. IL-6 and HLA-DR are abundantly expressed in M1-polarized monocytes and are widely accepted markers of M1 polarization.⁶⁶ Moreover, both are relevant markers within the context of neuroinflammation in diseased states. For example, elevated levels

of HLA-DR have been observed in the brains of Multiple Sclerosis patients.⁶⁷ Also, IL-6 expression is positively correlated with both seizure frequency and severity.⁶⁸ THP1 cells were dosed with LPS for 24 hours. We detected changes in IL-6 and HLA-DR protein expression levels, probed using western blots (Fig. 3.1). Expression levels were normalized to the housekeeping gene heat shock protein 60 (HPS60), that served as a loading control, and then also normalized to the control group that received no LPS. Because 10 ng/mL LPS maximized IL-6 expression and increased average HLA-DR expression in THP1 monocytes, it was selected as the working LPS dose for subsequent experiments to create an inflammatory response.

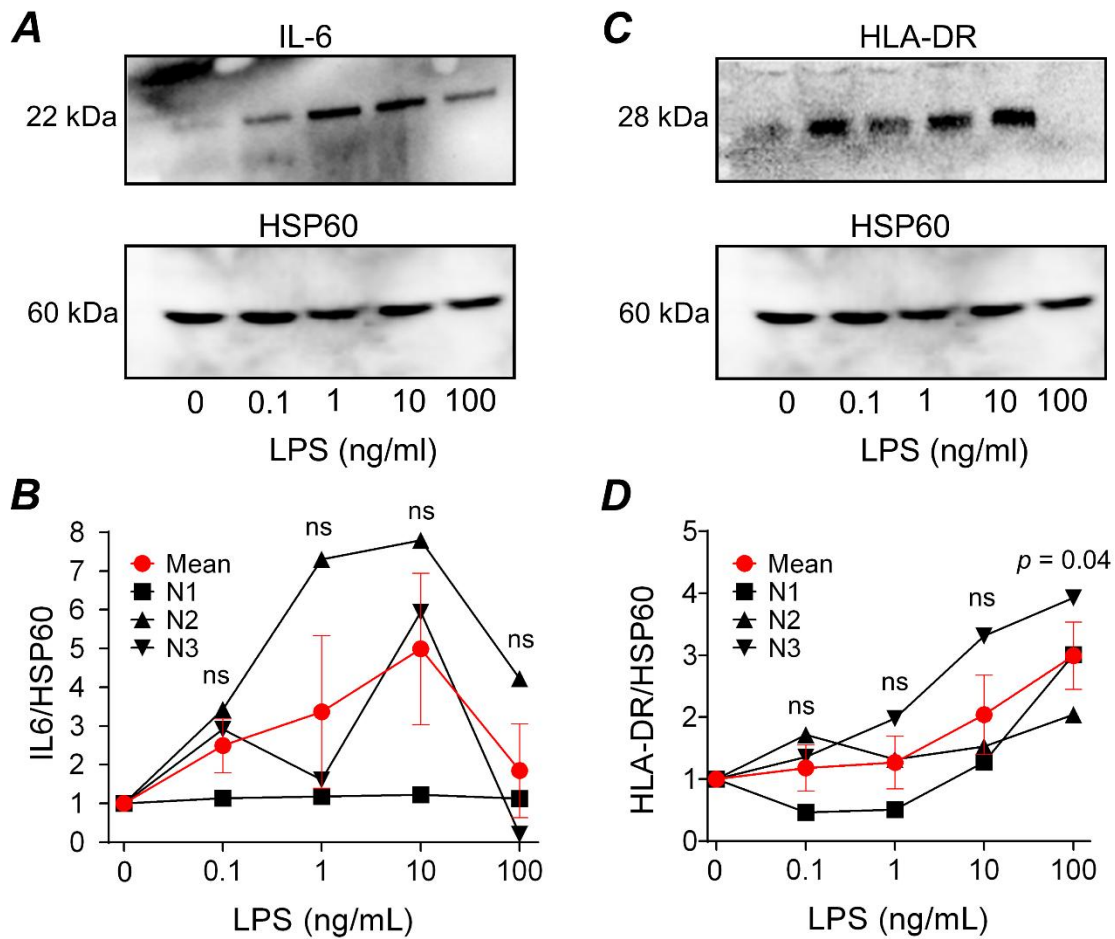


Figure 3.1.1: Western blot images measuring the change in IL-6 (A, B) and HLA-DR (C, D) protein expression in response to different doses of LPS within 24 hours. Expression levels are normalized to HSP60 which serves as the loading control and subsequently normalized to the no LPS treatment group. LPS doses were compared to no LPS treatment using a one-way ANOVA with Sidak's posthoc test. Data is considered statistically significant if $p < 0.05$. All biological replicates were collected from separate passages.

To evaluate how representative our in-vitro model of neuroinflammation pathway progression is, we sought to verify that the observed inflammatory response was a direct consequence of LPS induction and that LPS was exclusively signaling through TLR4. To do this, THP1 cells were pre-treated with TAK-242, a TLR4 inhibitor (also known as CP-690,550), at a concentration of 10 μ M before being treated and incubated with 10 ng/mL of LPS for 24 hours.

TAK-242 is a non-competitive inhibitor that covalently modifies a key cysteine residue on the intercellular domain of TLR4.⁶⁹ This covalent modification prevents adaptor proteins like MyD88 from associating with the intracellular domain of the receptor, thereby blocking the progression of the pro-inflammatory pathway seen in Figure 1.4.⁶⁹ Protein expression levels of IL-6, phosphorylated nuclear factor kappa B (NFkB), and phosphorylated IκB kinase (IKK) were probed via western blot. If LPS is exclusively signaling through TLR4, then TAK-242 should block downstream phosphorylation of NFkB and IKK, consequently also blocking IL-6 induction. Treatment of THP1 monocytes with the TLR4 inhibitor blocked any induction of IL-6, phosphorylated NFkB, and phosphorylated IKK, maintaining expression of all 3 markers at basal levels, comparable to the control group (Fig. 3.2).

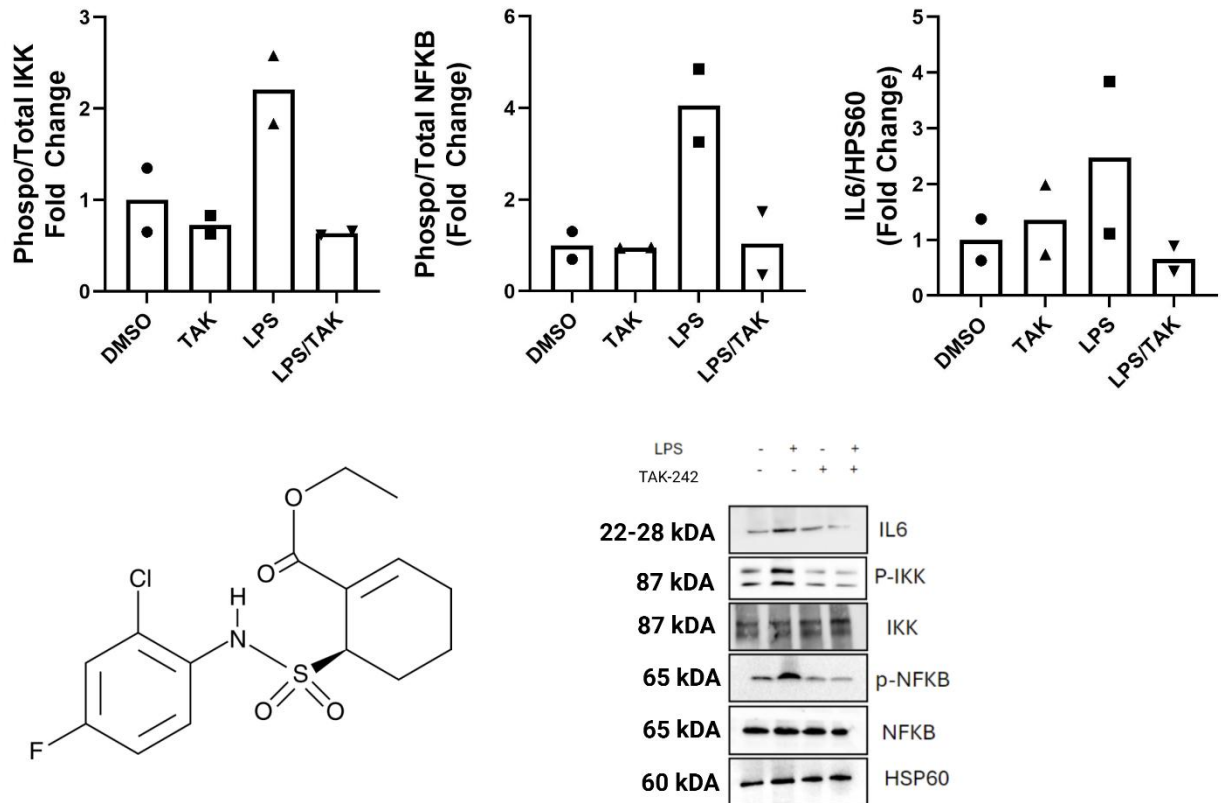


Figure 3.1.2: Western blot images measuring the change in Phosphorylated NFKB (A), Phosphorylated IKK (B), and IL-6 (C). Changes in phosphorylated protein are calculated by normalizing obtained quantification values to a loading control, HPS60. Phosphorylated protein band intensities are then divided by corresponding total protein intensities and the normalized to the average of the control groups (DMSO-treated) — Both N1 and N2 were run on the same blot. IL-6 was quantified by normalizing band intensity to the HSP60 loading control and then normalizing value for all treatment groups to the average of the control group to obtain a fold change. All biological replicates were collected from separate passages.

3.2 The Effect of CP-690,550 on Inflammatory Cytokine mRNA Transcription in THP1 Monocytes

Having established an in-vitro model for inflammation, the ability of CP-690,550 to prevent LPS-induced inflammation was then investigated. As previously mentioned, many different cell populations, both originating from the brain and originating from the peripheral immune system, contribute to neuroinflammation. THP1 monocytes, a population of human-

derived peripheral immune cells, were pre-treated with CP-690,550 for two hours before exposure to 10 ng/mL of LPS for an additional two hours. The dose range for CP-690,550 was selected based on the reported cell IC_{50} in the original synthesis paper which found 11 nM was sufficient to prevent IL-2-dependent proliferation of primary T-cells.⁵⁹ qRT-PCR was then used to probe the fold change in mRNA levels for 4 different inflammatory mediators (COX-2, CCR2, CD80 and IL-6), relative to the control group. We found that LPS exposure resulted in a change in the mRNA of all four mediators, but Tofacitinib failed to reverse the effect of LPS (Fig. 3.2).

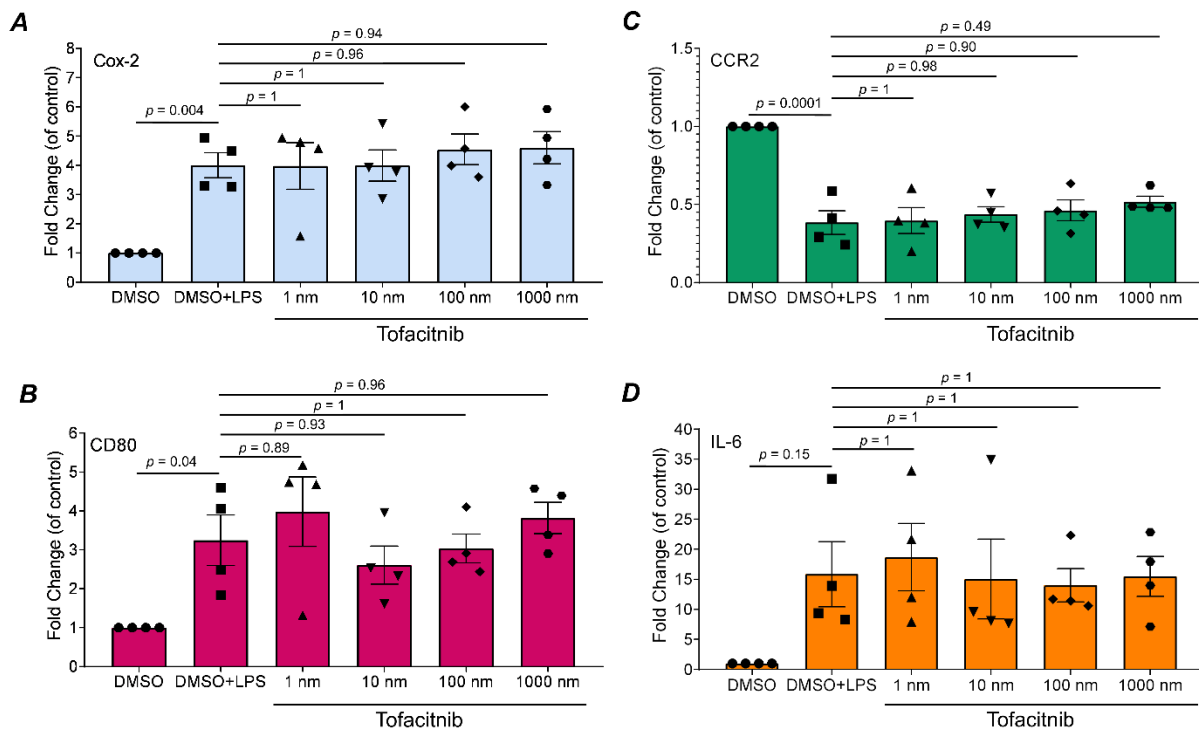


Figure 3.2 mRNA fold changes of Cox-2, CCR2, IL-6, and CD80 in THP1 monocytes treated with varying concentrations Tofacitinib and 10 ng/mL of LPS. Tofacitinib doses were compared to the DMSO + LPS treatment using a one-way ANOVA with Sidak's posthoc test with selected pairs. Data is considered statistically significant if $p < 0.05$. Bars represent the mean and SEM ($n = 4$ independent experiments). Each experiment was collected from separate passages.

3.3: The Effect of CP-690,550 on Inflammatory Cytokine mRNA in BV2-EP2 Cells

To determine if the lack of a CP-690,550-induced reduction of inflammatory mediators within the 1 nM-1000 nM dose window is cell-specific, we investigated the effect of LPS and CP-690,550 treatment in a mouse microglia cell line. Microglia are another cell population that contributes to neuroinflammation via a similar but distinct mechanism. LPS induced a more robust inflammatory response in BV2-EP2 microglia compared to THP1 monocytes (Fig. 3.3.1).

Similar to THP1 monocytes, CP-690,550 failed to inhibit the induction of IL-1 β and TNF- α . The COX-2 enzyme, another inflammatory marker downstream of TLR4 was also unaffected. No visual trend in the average fold change of IL-1 β , TNF- α , or Cox-2 was detected (Fig 3.3.1). The lack of a dose-dependent change in these 3 inflammatory mediators was also seen represented in the slopes of each dose-dependent curve and they did not statistically differ from 0 in a simple linear regression (Fig 3.3.2).

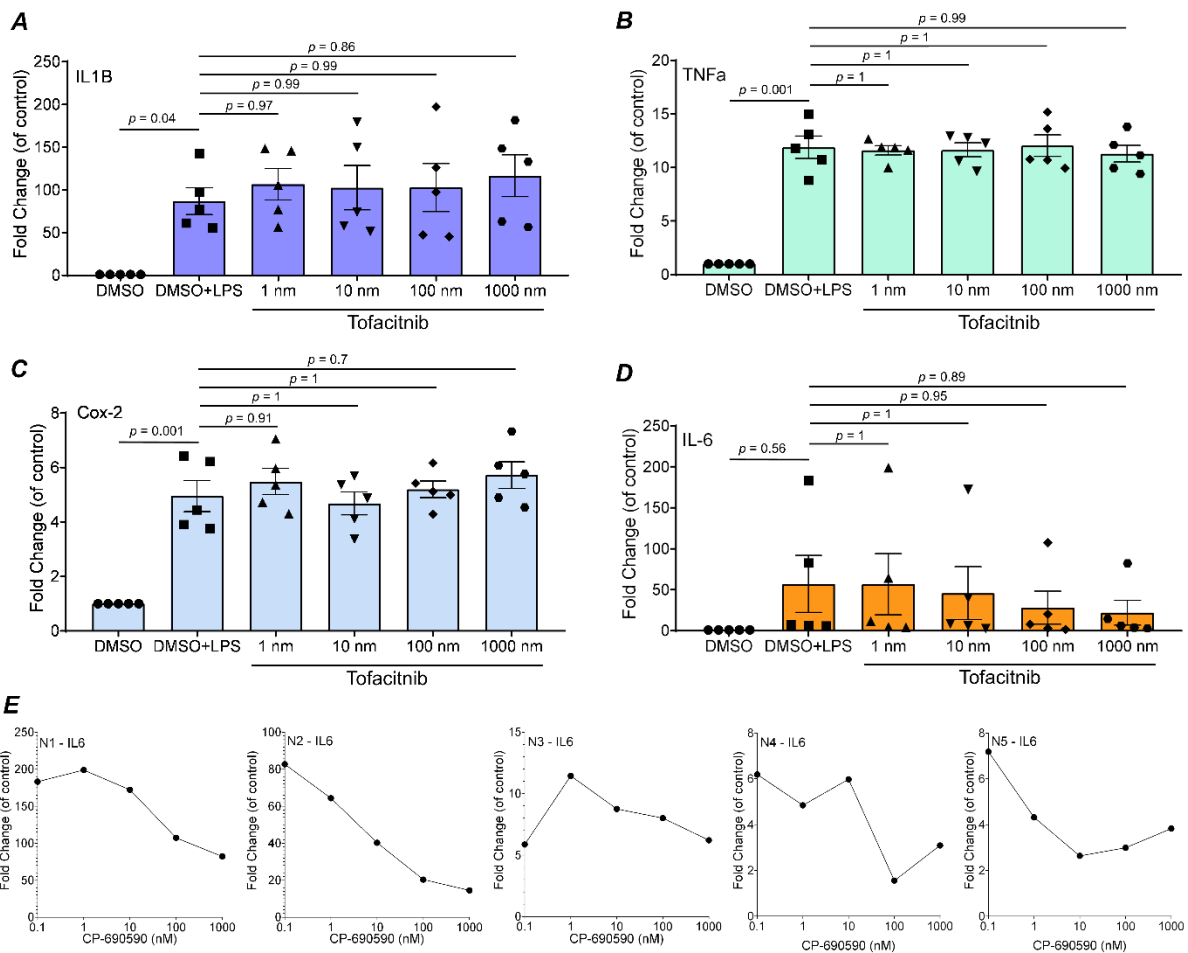


Figure 3.3.1: mRNA fold changes of IL-1 β (A), TNF- α (B), Cox-2 (C), and IL-6 (D) in BV2-hEP2 cells treated with different concentration Tofacitinib and 10 ng/mL of LPS, calculated relative to the amount of RNA found in the control samples using the $2\Delta\Delta CT$ method. (E) Shows modulation of IL-6 expression as Tofacitinib increases across all 4 biological replicates. Tofacitinib doses were compared to the DMSO + LPS treatment using a one-way ANOVA with Sidak's posthoc test with selected pairs. Data is considered statistically significant if $p < 0.05$. Bars represent the mean and SEM ($n = 5$ independent experiments). Each experiment was collected from separate passages.

Despite the variability also displayed in the IL-6 expression data, IL-6 was suppressed in a dose-dependent manner across 4 of the 5 trials (Fig 3.3.1). When the average IL-6 fold changes across the different doses are subjected to a simple linear regression, a slope of -0.2145 is obtained that is statistically significant ($P=0.0153$) (Fig. 3.3.2). The associated R^2 is 0.9696, indicating that the variability in average IL-6 expression is strongly dependent on the dose of CP-690,550.

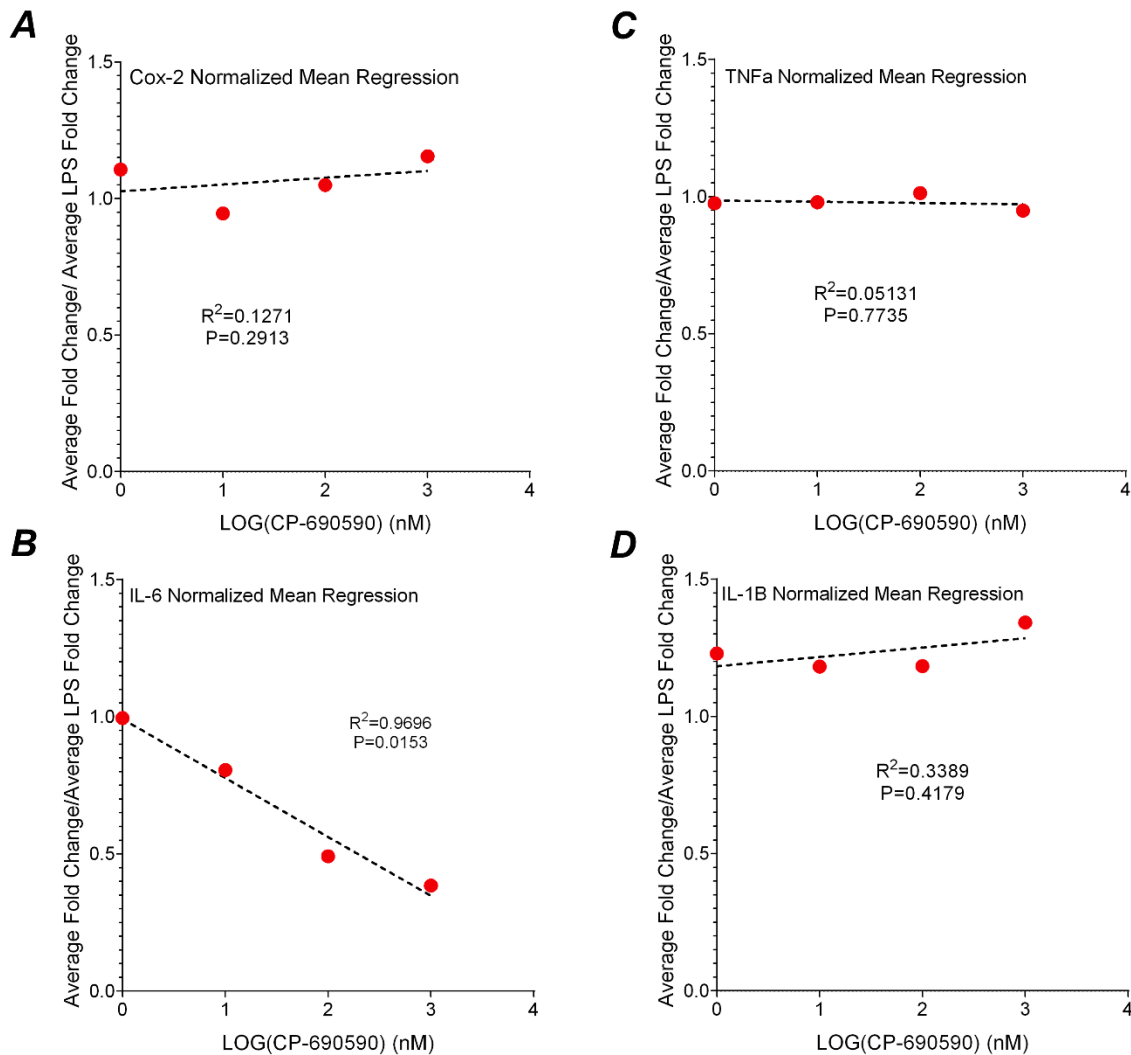


Figure 3.3.2: Average fold changes corresponding to different concentrations of CP-690,550 were normalized to the marker fold changes of LPS-treated group. A simple linear regression was then run on these averages for each marker and the slope, its corresponding p-value, and the R-squared were calculated for each inflammatory marker. A normalized fold change greater than 1 indicates increased expression with Tofacitinib treatment relative to the LPS-treated group. A normalized fold change below 1 indicates inhibition of the inflammatory mediator.

3.4 BV2-EP2 Mouse Primer Validation

qRT-PCR primer validation was conducted to confirm the quality of each primer, correct pipetting techniques and quality of sample and SYBR green. We identified the linear range of

detection for each primer set and ensure the concentration of cDNA being used in the qRT-PCR reactions was in the linear range. A dilution series of cDNA from cells treated for 2 hours with LPS was used with dilution factors ranging from 1/10 to 1/10000. PCR efficiency quantifies the efficiency of amplification within the reaction and is defined by the equation below.⁷⁰

$$PCR\ Efficiency = E = (10^{1/slope} - 1) \times 100$$

If the qRT-PCR was 100% efficient, the amount of cDNA should double in each cycle.⁷¹ To determine how many qRT-PCR cycles it would take for the 1/100 diluted sample of cDNA to achieve the same amount of cDNA in the 1/10 diluted sample, the following equation can be used.

$$2^n = 10$$

$$n \log 2 = \log 10$$

$$n \approx 3.3$$

It would take the 1/100 diluted cDNA 3.3 more qRT-PCR cycles to achieve a given threshold value of cDNA than the 1/10 diluted cDNA. Hence, a standard curve cDNA in a ten-fold dilution series should possess a slope of 3.3 if the qRT-PCR was 100% efficient. Practically, optimal experimental efficiency lies between 90% and 110%.⁷¹ If the slope is lower than 3.3, it will generate a qRT-PCR efficiency that is higher than 100%. The lower the slope, the less cycles it takes for the reaction to generate the threshold amount of cDNA. If the dilutions are normalized to the geometric mean of the CT values of 3 housekeeping genes, a line with a slope near 0 should emerge. Efficiencies outside of the acceptable range may be due to polymerase inhibition, non-specific primer binding, or contamination. They also may indicate a departure from the linear range of detection for the given primer.^{70,71} When a departure is observed, the upper and lower Ct (Cq) values that are interpretable can be defined.⁷⁰ Linear standard curves were detected for all primer

sets used for the inflammatory mediators (Fig. 3.4). Linear regression analysis revealed a positive correlation with the dilution factor of the primers and the CT value for each gene of interest measured (Fig. 3.4).

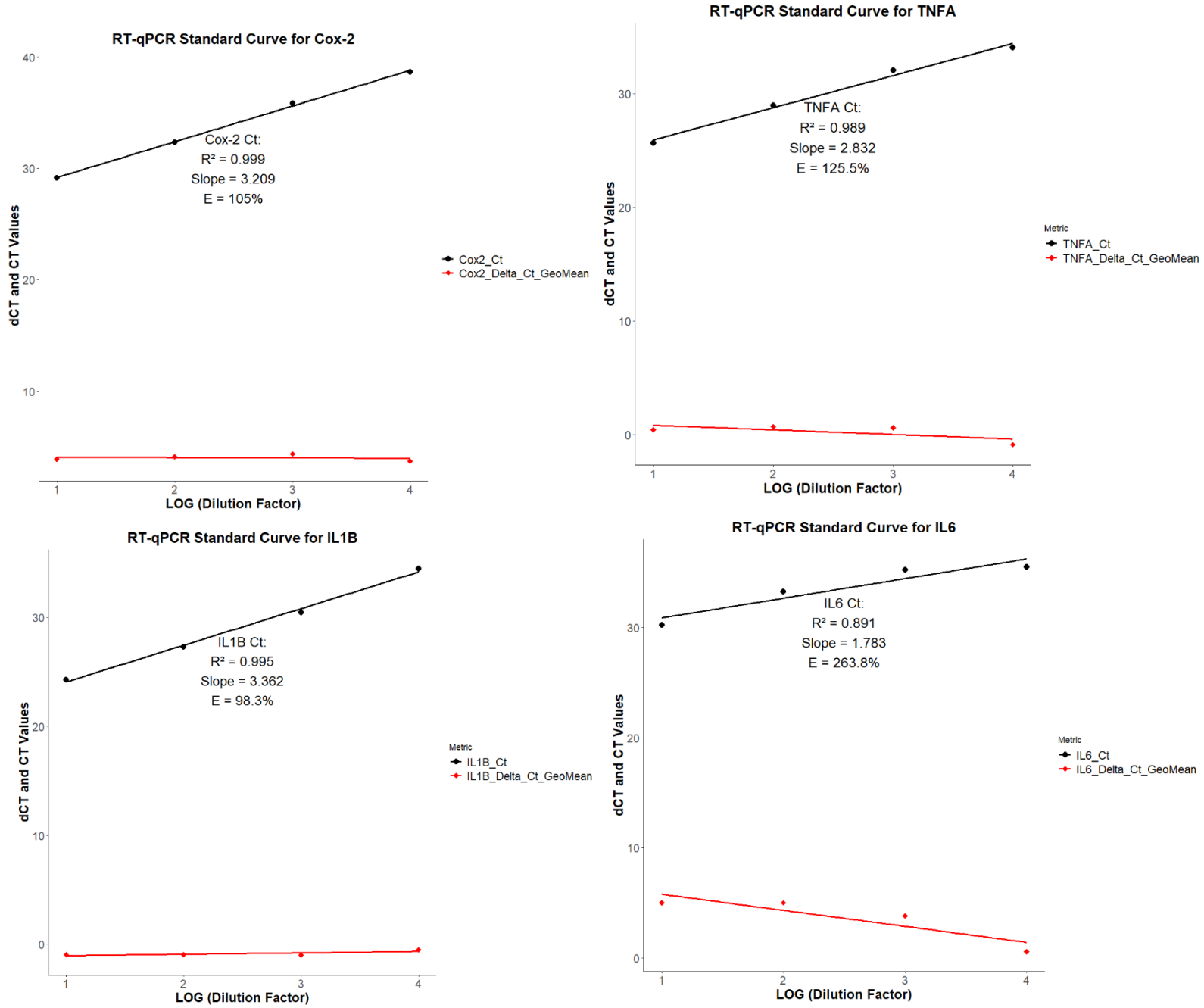


Figure 3.4: Standard curves for mouse primers used in the qRT-PCR reactions in the measurement of mRNA of Cox-2, TNF- α , IL-1 β , IL-6. The black line represents the change in CT values across increasingly diluted cDNA from the same sample of LPS-treated cells. The red line plots the dCT values, normalizing to the geometric mean of Housekeeping genes: Actin, GAPDH, and HPRT.

3.5 The Effect of CP-690,550 on STAT3 phosphorylation in BV2-hEP2 cells

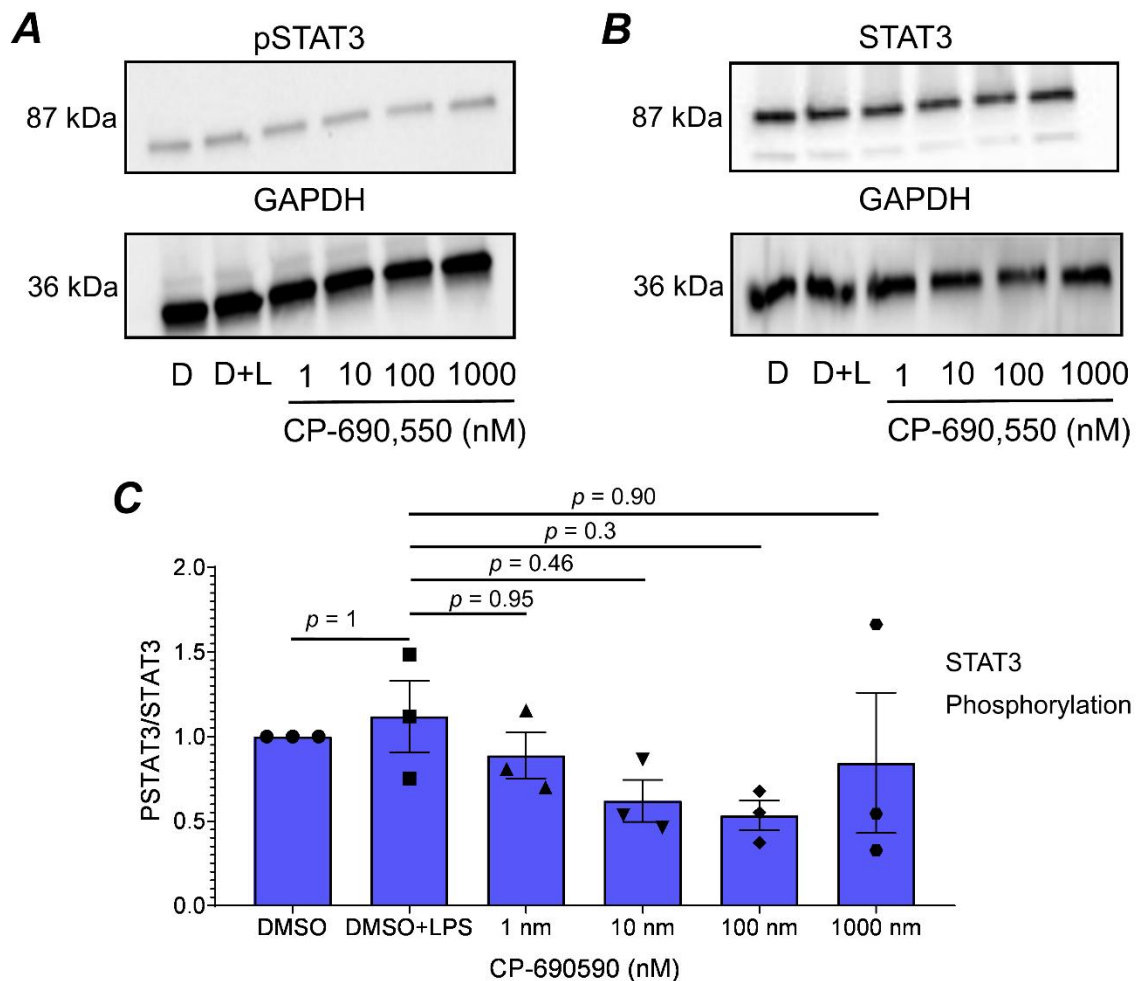


Figure 3.5.1: Western blot fold changes of pSTAT3 (A) and STAT3 (B) in BV2-hEP2 cells treated with different concentration Tofacitinib and 10 ng/mL of LPS. C, shows change in expression of phosphorylated STAT3 as a function of total STAT3 as CP690590 increases across all 3 biological replicates. CP690590 doses were compared to the DMSO + LPS treatment using a one-way ANOVA with Sidak's posthoc test with selected pairs. Data is considered statistically significant if $p < 0.05$. Bars represent the mean and SEM (n = 3 independent experiments). Each experiment was collected from separate passages.

Tofacitinib's lack of inhibition of the inflammatory mediators could be due to a dose range that is insufficient to block JAK activation in the selected cell-lines. Alternatively, qRT-PCR measures the relative mRNA levels of genes of interest. Due to additional layers of transcriptional

and translational regulation, changes in mRNA transcript levels do not always correlate with corresponding protein expression levels. Hence, it is pertinent to probe whether the drug is affecting protein expression levels of the inflammatory mediators.

To determine whether the selected dose range was sufficient to block JAK activation, western blot was conducted to probe the levels of STAT3 phosphorylation when exposed to LPS in the presence of different doses of Tofacitinib after 24 hours. STAT3 phosphorylation occurs directly downstream of JAK phosphorylation, serving as an indication of the activation of the pathway following LPS exposure. LPS induction for 24 hours did not appear to show a significant change in STAT3 phosphorylation with an average fold change in phosphorylation of 1.11, relative to the DMSO group (Fig. 3.5.1). Despite the lack of LPS induced STAT3 phosphorylation, CP-690,550 appears to suppress the existing phosphorylation of STAT3 in a dose-dependent manner (Fig. 3.5.1).

To determine whether LPS induced a response that differed from control DMSO treated cells, western blot was performed using the same samples to probe for IL-1 β , a cytokine whose expression upon activation is sustained for longer periods. The average fold change for IL-1 β across all treatment groups was standardized to GAPDH loading controls and then normalized to the control DMSO treatment group revealed only a slight change in IL-1 β expression over the 24-hour time period (Fig. 3.5.2).

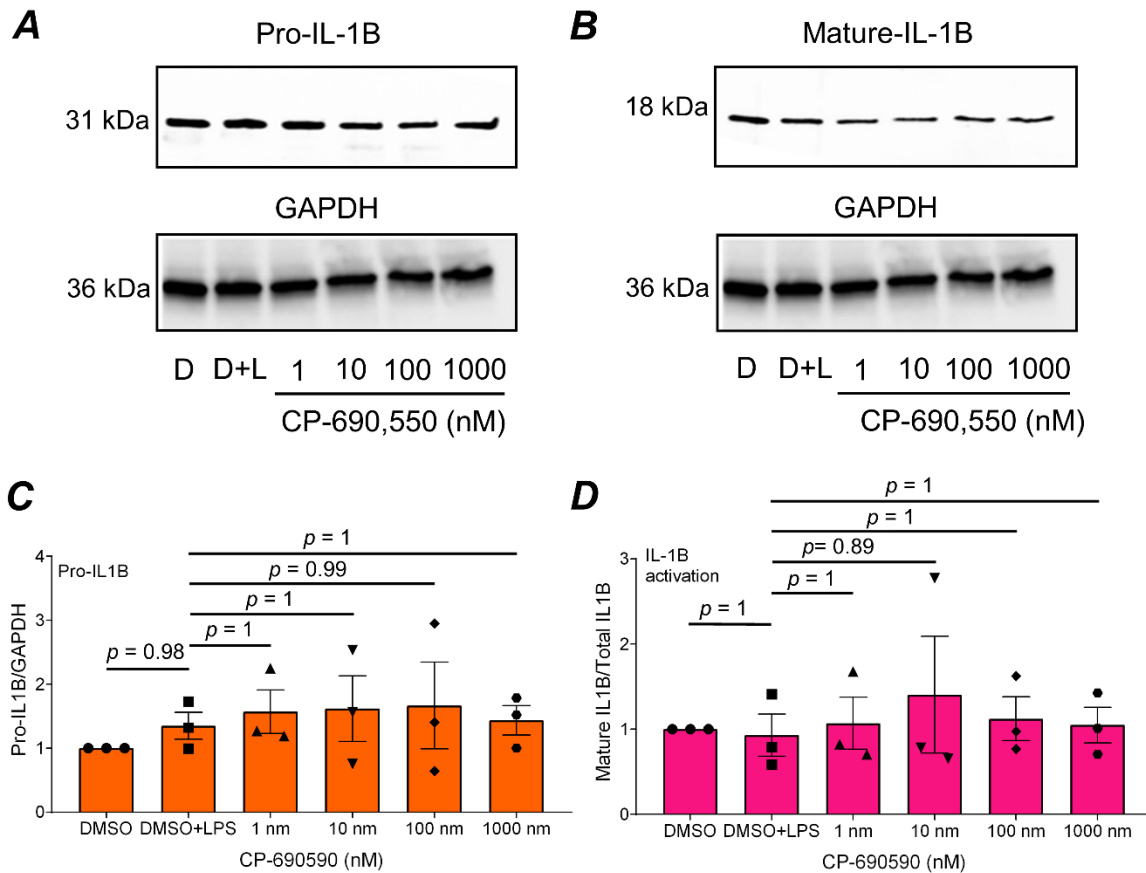


Figure 3.5.2. Western blot fold changes of pro-IL-1 β (A, C) and mature IL-1 β (B, D) in BV2-hEP2 cells treated with different concentration CP690590 and 10 ng/mL of LPS. Shows change in expression of phosphorylated STAT3 as CP690590 increases across all 3 biological replicates. CP690590 doses were compared to the DMSO + LPS treatment using a one-way ANOVA with Sidak's posthoc test with selected pairs. Data is considered statistically significant if $p < 0.05$. Bars represent the mean and SEM ($n = 3$ independent experiments). Each experiment was collected from separate passages.

In the LPS-treated group, a slight induction in the average of pro-IL-1 β of a 1.7-fold increase relative to the DMSO was detected (Fig. 3.5.2). The lack of a more robust change in IL-1 β expression, in combination with the lack phosphorylated STAT induction, suggests there may be an exogenous source of inflammation induction in the media or elsewhere in the cellular environment. Regardless, unlike with phosphorylated STAT3, the application of the inhibitor did not quench pro-IL-1 β expression, matching the RNA-level expression observed in the qRT-PCR

results (Fig.3.5.2). As expected, the average levels of activated cleaved IL-1 β were not increased by LPS (Fig.3.5.2). It has been established that LPS alone can increase IL-1 β expression but not activation.⁷² Caspase-1 facilitates the cleavage and consequential activation of IL-1 β and requires secondary stimulation.⁷²

4. Discussion

4.1 Despite variability in response across the biological replicates, 10 ng/mL of LPS induced a maximal response in IL-6 elevation. Interestingly, increasing the LPS dose to 100 ng/mL led to a decline in IL-6 expression, relative to the 10 ng/mL treatment group, across all three biological replicates. This is in contrast to HLA-DR expression which tends to continuously increase, peaking at the 100 ng/mL dose. The decrease in IL-6 at the 100 ng/mL dose may be attributed to the excess stress or damage caused by constant exposure to LPS, which is cytotoxic at high doses.⁷³ This stress may trigger other pathways that counteract IL-6 induction while leaving the HLA-DR response intact. Alternatively, the IL-6 expression induced by 100 ng/mL of LPS may be quenched by a negative feedback mechanism. Endogenous SOCS (Suppressor of Cytokine Signaling) inhibits hyperactivity of the JAK-STAT pathway by blocking JAK phosphorylation and is induced by cytokines including but not limited to IL-6, IFN- γ , and IL-4.⁷⁴ LPS induces SOCS-1 expression. Importantly, while SOCS-1 has been shown to inhibit LPS-induced IL-6 expression, SOCS has not been shown to affect levels of HLA-DR.^{75,76} LPS (100 ng/mL) may have increased IL-6 expression to such an extent that it induced SOCS, leading to a decrease in the observed induction after 24 hours. To confirm this hypothesis, a western blot probing SOCS-1 level is needed. Regardless, because 10 ng/mL LPS maximized IL-6 expression and increased average HLA-DR

expression in THP1 monocytes, it was selected as the working LPS dose for subsequent experiments to create an inflammatory response.

4.2 IL-6, CD80, Cox-2, and CCR2 are all established markers for M1 polarization. IL-6 is a cytokine, Cox-2 is an enzyme, CD80 is a glycoprotein, and CCR2 is a chemotactic receptor found on monocytes and macrophages that controls migration to the site of inflammation. As shown in Figure 3.2, LPS increased the fold change for IL-6, CD80, and Cox-2, aligning with LPS induction as a model for neuroinflammation. Conversely, LPS shows a decrease in CCR2 mRNA. This does not align with the neuroinflammation model as the upregulation of CCR2 in monocytes facilitates their migration and infiltration into the epileptic brain. During in-vivo inflammatory events CCR2 is upregulated. This incongruous in-vitro decrease coincides with previous literature which shows that LPS does not decrease the rate of mRNA transcription but rather decreases the stability of the transcribed mRNA.⁷⁷

Nevertheless, CP-690,550 did not affect the average mRNA levels of any of the screened markers at any dose. In two of the four trials, IL-6 mRNA transcription did decrease at the 1000 nM dose. However, the reduction was slight and failed to manifest in the other two biological replicates. The lack of effect could indicate that a higher dose is required to inhibit the production of the screened markers. The doses tested were chosen in this study based on the reported amount of Tofacitinib required to inhibit 50% of IL-2-dependent proliferation in T cells (11 nM). Previous studies that screened Tofacitinib, in different cell lines and against different agonists, found the drug was effective at decreasing the production of pro-inflammatory mediators at different concentrations. While some studies use concentrations on a micromolar scale, several studies found a reduction of pSTAT1 and pSTAT3 at lower concentrations of CP-690,550. For example,

in THP1 monocytes, it was determined that both 500 nM and 2000 nM of CP-690,550 decreased pSTAT1 expression that was elevated by IFN γ .⁷⁸ In patient-derived fibroblast-like synoviocytes, CP-690,550 inhibited 50% of IL-6-induced phosphorylation at concentrations of 23 nM and 77 nM.⁷⁹ In Mouse-derived CD4+ T cells, in a dose curve ranging from 0 nM to 1000 nM, Tofacitinib doses of 300 nM and 1000 nM both significantly decrease phosphorylation of STAT1 and STAT3.⁸⁰ Slight inhibition was also observed at 100 nM.⁸⁰ In whole human blood assay, IFN- γ was inhibited by Tofacitinib with IC₅₀= 121 nM.⁸¹ In contrast, another paper that treated THP1 cells differentiated by PMA with a single 10 μ M dose of Tofacitinib for 24 hours found a modest reduction of IL-6 but no reduction of TNF following LPS treatment.⁸² In a co-culture with BV2 microglia and neurons, 30 μ M, 60 μ M, and 90 μ M manifested a significant suppression of IL-6 and IL-1 β mRNA expression at all doses.⁸³ Again, like in our study, TNF- α showed no minimal changes in expression levels across treatment groups.⁸³ These concentrations were chosen due to the lack of cytotoxic effects displayed by BV2 and primarily microglia cells up to a concentration of 100 μ M.⁸³ Putting our results in the context of these prior studies, we cannot conclude that Tofacitinib fails to alter transcription activities of THP1 monocytes, altogether. Instead, further studies must be conducted with an expanded dose range with concentrations in the micromolar range.

4.3 Prior studies performed in different contexts have demonstrated CP-690,550's selective suppression of IL-6 and not IL-1 β . Daily administration of Tofacitinib in rat adjuvant-induced arthritis models showed that IL-6 suppression occurred within 4 hours after the animals received their first dose. In contrast, levels of IL-1 β mRNA showed no significant difference until the 7th day of treatment.⁸⁴ In another study, peripheral blood mononuclear cells (monocytes) obtained

from arthritis patients and dosed with Tofacitinib at concentrations ranging from 0 to 100 micromolar in-vitro for 6 hours observed a significant reduction in IL-6 but hardly any changes in IL-1 β .⁶⁴ In fact, they present a dose curve for IL-1 β with a slope that is similar to the one in Figure 3.3.2. The same study also found that the effects of Tofacitinib on different cytokines differ between cell types. Synoviocytes (macrophages that line the joint capsule) did not show the same reduction of IL-6 that the monocytes did.⁶⁴ This demonstrates that, although mechanisms of cytokine productions across cell-type may be similar, signaling landscapes are not identical. Hence, inhibition of IL-6 in BV2-hEP2 microglia and not THP1 monocytes is possible.

A different prior study demonstrated that AG-490, a JAK-2 inhibitor blocked hydrogen peroxide-induced JAK-2 activation and subsequent Cox-2 and INOS elevation.⁸⁵ An additional study found that JAK3 inhibition via the WHI-P154 had no effect on Cox-2 and only manifested effects on TNF- α at 30 μ M.⁸⁶ Our experiments in the current study found that the dual inhibition of JAK3 and JAK1 by Tofacitinib also does not inhibit Cox-2 or TNF- α between the doses of 1 nM and 1 μ M. Hence it is possible that Cox-2 inhibition is only associated with JAK2. Moreover, higher doses of Tofacitinib may be needed to observe TNF- α inhibition.

The signal transduction of select cytokines, including IL-6, IL-23, IL-21, IL-12, and IFN γ all directly involve the phosphorylation of JAKs that reside at the receptor tails of these cytokine's receptors.³⁹ Transduction of IL-1 β does not predominantly signal through JAK phosphorylation.⁸⁷ CP-690550's suppression of IL-6 transcription but not IL-1 β may perhaps be explained by these differences in transduction mechanisms. IL-6 induction increases IL-6 transcription. IL-6 transduction phosphorylates and activates STAT3 and NF κ B which synergistically increase IL-6 production.⁸⁸ Since IL-6 transduction is directly facilitated by JAK1, inhibition of JAK1 inflicted by Tofacitinib may interrupt this positive feedback loop, manifesting in the observed suppression

of IL-6 transcription. While IL-1 β engages in a positive feedback loop of similar fashion, the IL-1 β receptors do not predominantly associate with a JAK. Instead, binding of IL-1 β to the IL-1 receptor recruits and complexes with a co-receptor chain (IL-1RAcP).^{87,89} This leads to the subsequent recruit of myeloid differentiation primary response gene 88 (MyD88) protein and interleukin-1 receptor-activated protein kinase (IRAK). Together, these components form a stable signaling module which, parallel to other phosphorylation events by different IRAK and MAPK subtypes, can lead to IL-1 β transcription via NF κ B, activator protein 1 (AP-1) signaling.^{87,89} Unlike IL-6, STAT as a transcription factor and, hence, JAK phosphorylation, is not predominantly involved in this positive feedback cycle. Hence, inhibition of JAK-activated STAT3 should not drastically impair it.

CP-690550's suppression of IL-6 transcription but not IL-1 β may also be attributed to the number of pathways that regulate the transcription of each cytokine and whether production is dominated by a process that is upstream or downstream JAK phosphorylation. Upon LPS activation, TLR4 complexes with the MyD88 adaptor protein. This is followed by recruitment and activation of the IL-1 receptor-associated kinase (IRAK) which subsequently complexes with and activates tumor necrosis factor (TNF)-associated factor 6 (TRAF6).^{90,91} At this level, several distinct signaling pathways branch out as TRAF6 activation can lead to several signal transduction pathways.^{90,91} Some of these pathways include the phosphatidylinositol 3-kinase (PI3K) pathway, the NF κ B pathway, and several MAPK pathways which include the c-Jun NH2-terminal protein kinase (JNK) pathway. Maximal IL-1 β expression is achieved early on, directly facilitated by LPS-induced NF κ B and JNK-activated AP-1.^{90,91} While NF κ B and AP-1 are also transcription factors for IL-6, transcription of IL-6 is perhaps maximized by STAT3. STAT3 exerts significant

control over IL-6 transcription; inhibition of STAT3 alone in primary glial cells reduces IL-6 transcription by 80%.⁹²

It is may also be possible that IL-6 suppression is enhancing IL-1 β signaling. A prior study conducted in co-cultures of astrocytes and microglia found that Si-RNA inhibition of LPS-induced IL-6 release consistently led to upregulated IL-1 β expression.⁹³ This study suggested that this may be due the fact that IL-6 inhibition downregulates SOCS-3 and IL-10 which would otherwise act to suppress IL-1 β .⁹³

Alternatively, blockage of the transduction of a cytokine that primarily signals through JAK3 may be selectively suppresses IL-6. While IL-4 is traditionally thought of as an anti-inflammatory marker, IL-4, in certain conditions, has been shown to sensitize macrophages to LPS, causing them to express more IL-6.⁹⁴ Moreover, in vascular endothelium, it has been show that IL-4 upregulates IL-6 mRNA and protein.⁹⁵ Here, it is possible that JAK3 inhibition may have blocked IL-4 transduction, decreasing that added IL-6 production.

Finally, similar to TNF- α , it is possible that higher doses of Tofacitinib (in the micromolar range), are needed to observe an inhibition of IL-1 β , relative to IL-6.

4.4 The standard curves for both the IL-1 β primers and the Cox-2 primers display near-optimal qRT-PCR efficiencies, indicating a large linear range of detection and good quality cDNA sample. IL-6 and TNF- α deviate from the optimal efficiencies. Examining the raw data values for TNF- α , the difference in CT values between the 1/10 dilution and the 1/100 dilution is 3.22. The CT value difference between the 1/100 and 1/1000 dilutions is 3.37. In contrast, the difference in CT values between 1/1000 dilution and 1/10,000 dilutions is 1.66. Hence, the slightly elevated TNF- α efficiency of 125.5% is likely skewed by the fact that the 1/10,000 dilution falls outside

the linear range. If the 1/10,000 data point is removed from the line, the calculated slope amongst the 3 points becomes 3.299 which would yield an efficiency of 101%. Hence the boundary of the linear range of detection for TNF- α can be established at the CT-value of 32.54. Any CT value that resides above this may not reflect an accurate change in gene expression. All the raw CT values obtained in the TNF- α qRT-PCR fall within the linear range, never exceeding a CT value of 32.4.

The calculated efficiency for the IL-6 qRT-PCR reactions is exorbitantly high at 263.8%. Removing the 1/10000 datapoint which visually appears to fall outside the linear range of detection results in a slope of 2.96 that yields an efficiency of 117%. With the identification of the linear range of detection, anything above the CT value of 36.2 is said to fall outside of the linear range of detection. All the raw CT values obtained in the IL-6 qRT-PCR fall within the linear range, never exceeding a CT value of 36.2. However, the revised calculated efficiency within the linear range of IL-6 qRT-PCR reactions still falls outside the optimal efficiency range. This suboptimal efficiency is likely not due to sample quality, reagent quality, or technique as all other reactions using different primers yielded optimal qRT-PCR efficiencies. Instead, this may be caused by IL-6 primer specificity or quality concerns. Hence, future repetitions of these experiments should consider using a different primer pair for IL-6.

4.5. The lack of observed LPS-induced STAT3 phosphorylation could be due to the incubation time with LPS. Phosphorylation is a rapid process and it is possible that the time to detect the peak LPS-induced phosphorylation occurred prior to the 24-hour time point and then subsequently subsided. That being said, the lack of a more robust change in IL-1 β expression, in combination with the lack phosphorylated STAT induction suggests there may be an exogenous source of inflammation induction in the media or elsewhere in the cellular environment.

Importantly, STAT3 phosphorylation is not entirely eliminated by JAK1/JAK3 inhibition. There are other kinases that can phosphorylate STAT, including src family kinases and receptor tyrosine kinases.⁹⁶ However, the failure to reduce average STAT3 phosphorylation by at least 50% across the three replicates, may suggest that higher doses of Tofacitinib are required to block JAK3/1 activation and observe modulation.

5. Conclusion and Future Directions

This study began by establishing a model for neuroinflammation in THP1 cells, using 10 ng/mL of LPS to induce a pro-inflammatory response of cells in-vitro. To confirm the robustness of our model, TAK-242, was used to verify that LPS was exclusively signaling through TLR4, whose activation is believed to occur very early on in epileptogenesis and facilitate the downstream pro-inflammatory feedback loops present in epilepsy.

Thereafter, Tofacitinib was found to have no effect on the transcription of pro-inflammatory mediators in THP1 monocytes between the doses of 1 nM to 1000 nM, failing to suppress mRNA levels of Cox-2, CCR2, CD80 and IL-6. This lack of transcription suppression may be due to an insufficient dose of Tofacitinib to inhibit JAK activation. Hence this study should be repeated to include micromolar doses of Tofacitinib.

It may also be possible that the observed effect of Tofacitinib in Hoffman et al. (2025) may not be due to an anti-inflammatory mechanism involving the screened mediators but rather may be acting to block immune cell proliferation via suppression of IL-2, IL-4, IL-7, IL-9, IL-15, and IL-21.⁹⁷ In future experiments, these cytokines should be screened to test this idea.

Furthermore, it could be that the reduction in seizure severity is due to a blockade of cytokine transduction on the neurons themselves. Recent evidence suggests that cytokine receptors are expressed on neurons, including IL-6 and TNF- α .^{98,99}

While Tofacitinib treatment in BV2-hEP2 similarly yielded no statistically significant differences in mRNA levels relative to BV2-hEP2 cells treated with LPS alone, all 4 trials demonstrate a dose-dependent decrease in IL-6, to various extents. The lack of statistical significance is, in part, due to variation in the extent of initial LPS induction and response. While variation could result from cell-culture conditions, we suspect it may be symptomatic of the primer quality and or specificity. Nonetheless, the consistent decrease in IL-6 is promising and may contribute to the larger explanation as to why Tofacitinib decreases seizure severity and frequency in kainite-induced epileptic mouse models. To verify this decrease, a western blot probing for IL-6 protein expression levels should be performed on samples treated in a similar manner. Like with THP1 cells, this experiment should also be repeated with an extended dose range.

The necessity for repetition of these experiments at a higher dose range is bolstered by our final experiment which showed that all doses of Tofacitinib failed to suppress STAT phosphorylation in a statistically significant manner.

In addition to expanding the dose range, treating both microglia and BV2-hEP2 and THP1 monocytes with siRNA to silence JAK3 may provide a more complete inhibition of JAK and allow us to probe downstream effects on inflammation with more clarity. In addition to collecting transcription and expression data via qRT-PCR and Western Blot, RNA-seq would allow us to survey the wider landscape of changing cellular pathways and perhaps uncover further markers of interest that may be contributing the overall reduction of seizures.

Lastly, it may be interesting to compare the effect of Tofacitinib in different glial cell populations such as astrocytes but also compare how the effects of Tofacitinib differ when applied to single cell populations versus cell populations that have been co-cultured (e.g. co-cultures of microglia and monocytes).

Study Limitations

There were limitations of this study. In the last experiment, it is suspected that there was source of exogenous inflammation due to the lack of induction of pro-inflammatory markers. Moreover, the quality of the IL-6 primers used to probe mRNA transcription in BV2-hEP2 may not have been optimal. Western blot was attempted to examine whether the suppression in IL-6 mRNA translated to the protein expression level. However, the IL-6 antibody failed to produce bands across several antibody concentrations and biological replicates. Moreover, the duration of each experiment set takes at least 4 weeks in order to wait for cells to reach total confluency, treat and collect the cells, extract the RNA and protein and then perform qRT-PCR and western blot and troubleshoot the relevant assays for all 4 replicates. Hence, this limited the amount of experiments that could be performed and the conditions that to be probed.

References

- (1) Vezzani, A.; Balosso, S.; Ravizza, T. Neuroinflammatory Pathways as Treatment Targets and Biomarkers in Epilepsy. *Nat. Rev. Neurol.* **2019**, *15* (8), 459–472. <https://doi.org/10.1038/s41582-019-0217-x>.
- (2) Hoffman, O. R.; Koehler, J. L.; Espina, J. E. C.; Patterson, A. M.; Gohar, E. S.; Coleman, E. M.; Schoenike, B. A.; Espinosa-Garcia, C.; Paredes, F.; Varvel, N. H.; Dingledine, R. J.; Maguire, J. L.; Roopra, A. S. Disease Modification upon 2 Weeks of Tofacitinib Treatment in a Mouse Model of Chronic Epilepsy. *Sci. Transl. Med.* **2025**, *17* (790), eadt0527. <https://doi.org/10.1126/scitranslmed.adt0527>.
- (3) Fisher, R. S.; Acevedo, C.; Arzimanoglou, A.; Bogacz, A.; Cross, J. H.; Elger, C. E.; Engel, J.; Forsgren, L.; French, J. A.; Glynn, M.; Hesdorffer, D. C.; Lee, B. I.; Mathern, G. W.; Moshé, S. L.; Perucca, E.; Scheffer, I. E.; Tomson, T.; Watanabe, M.; Wiebe, S. ILAE Official Report: A Practical Clinical Definition of Epilepsy. *Epilepsia* **2014**, *55* (4), 475–482. <https://doi.org/10.1111/epi.12550>.
- (4) Stafstrom, C. E.; Carmant, L. Seizures and Epilepsy: An Overview for Neuroscientists. *Cold Spring Harb. Perspect. Med.* **2015**, *5* (6), a022426–a022426. <https://doi.org/10.1101/cshperspect.a022426>.
- (5) Bromfield, E.; Cavazos, J. E.; Sirven, J. Chapter 1-Basic Mechanisms Underlying Seizures and Epilepsy. In *An Introduction to Epilepsy*; American Epilepsy Society: West Hartford (CT), 2006.
- (6) Alberts, B.; Johnson, A.; Lewis, J.; Raff, M.; Roberts, K.; Walter, P. Ion Channels and the Electrical Properties of Membranes. In *Molecular biology of the cell*; Garland Science: New York, 2002.
- (7) Bean, B. P. The Action Potential in Mammalian Central Neurons. *Nat. Rev. Neurosci.* **2007**, *8* (6), 451–465. <https://doi.org/10.1038/nrn2148>.
- (8) Kuriyan, J.; Konforti, B.; Wemmer, D. THE TRANSMISSION OF ACTION POTENTIALS IN NEURONS. In *The molecules of life: physical and chemical principles*; Garland Science, Taylor & Francis Group: New York, 2013. <https://doi.org/10.1201/9780429258787>.
- (9) Snutch, T.; Peloquin, J.; Mathews, E.; McRory, J. Molecular Properties of Voltage-Gated Calcium Channels. In *Madame Curie Bioscience Database*; Landes Bioscience: Austin (TX), 2000.
- (10) Purves, A.; Fitzpatrick, D. Excitatory and Inhibitory Postsynaptic Potentials. In *Neuroscience. 2nd edition.*; Sinauer Associates: Sunderland (MA), 2001.

- (11) Ariyo, O.; Akter, F. Anatomy and Physiology of the Neuron. In *Neuroscience for neurosurgeons*; Emptage, N., Engert, F., Berger, M. S., Eds.; Cambridge University Press: Cambridge, 2023.
- (12) Qiao, X.; Yao, W. Effect of Calcium on the Characteristics of Action Potential Under Different Electrical Stimuli. *AppliedMath* **2024**, *4* (4), 1358–1381. <https://doi.org/10.3390/appliedmath4040072>.
- (13) Abbaszadeh, B.; Teixeira, C. A. D.; Yagoub, M. C. E. Online Seizure Prediction System: A Novel Probabilistic Approach for Efficient Prediction of Epileptic Seizure with iEEG Signal. *Open Biomed. Eng. J.* **2022**, *16* (1), e187412072208300. <https://doi.org/10.2174/18741207-v16-e2208300>.
- (14) Salter, M.; Dong, Y.; Kalia, L.; Liu, X. J.; Pitcher, G.; VanDongen, A. M. J. Chapter 7 Regulation of NMDA Receptors by Kinases and Phosphatases. In *Biology of the NMDA receptor*; Frontiers in neuroscience; CRC press: Boca Raton (Fla.), 2009.
- (15) Isaac, J. T. R.; Ashby, M. C.; McBain, C. J. The Role of the GluR2 Subunit in AMPA Receptor Function and Synaptic Plasticity. *Neuron* **2007**, *54* (6), 859–871. <https://doi.org/10.1016/j.neuron.2007.06.001>.
- (16) Gorter, J. A.; Zurolo, E.; Iyer, A.; Fluiter, K.; Van Vliet, E. A.; Baayen, J. C.; Aronica, E. Induction of Sodium Channel Na_x (*SCN7A*) Expression in Rat and Human Hippocampus in Temporal Lobe Epilepsy. *Epilepsia* **2010**, *51* (9), 1791–1800. <https://doi.org/10.1111/j.1528-1167.2010.02678.x>.
- (17) Kaplan, D. I.; Isom, L. L.; Petrou, S. Role of Sodium Channels in Epilepsy. *Cold Spring Harb. Perspect. Med.* **2016**, *6* (6), a022814. <https://doi.org/10.1101/cshperspect.a022814>.
- (18) Su, H.; Sochivko, D.; Becker, A.; Chen, J.; Jiang, Y.; Yaari, Y.; Beck, H. Upregulation of a T-Type Ca²⁺ Channel Causes a Long-Lasting Modification of Neuronal Firing Mode after Status Epilepticus. *J. Neurosci.* **2002**, *22* (9), 3645–3655. <https://doi.org/10.1523/JNEUROSCI.22-09-03645.2002>.
- (19) Lerche, H.; Shah, M.; Beck, H.; Noebels, J.; Johnston, D.; Vincent, A. Ion Channels in Genetic and Acquired Forms of Epilepsy. *J. Physiol.* **2013**, *591* (4), 753–764. <https://doi.org/10.1113/jphysiol.2012.240606>.
- (20) Maguire, J. Epileptogenesis: More Than Just the Latent Period. *Epilepsy Curr.* **2016**, *16* (1), 31–33. <https://doi.org/10.5698/1535-7597-16.1.31>.
- (21) Patel, D. C.; Tewari, B. P.; Chaunsali, L.; Sontheimer, H. Neuron–Glia Interactions in the Pathophysiology of Epilepsy. *Nat. Rev. Neurosci.* **2019**, *20* (5), 282–297. <https://doi.org/10.1038/s41583-019-0126-4>.

- (22) Vezzani, A.; French, J.; Bartfai, T.; Baram, T. Z. The Role of Inflammation in Epilepsy. *Nat. Rev. Neurol.* **2011**, *7* (1), 31–40. <https://doi.org/10.1038/nrneurol.2010.178>.
- (23) Vezzani, A.; Balosso, S.; Ravizza, T. The Role of Cytokines in the Pathophysiology of Epilepsy. *Brain. Behav. Immun.* **2008**, *22* (6), 797–803. <https://doi.org/10.1016/j.bbi.2008.03.009>.
- (24) Rosch, R. E.; Samarut, É. Epileptic Seizures: Glia–Neuron Interactions For Better or For Worse. *Curr. Biol.* **2019**, *29* (23), R1248–R1251. <https://doi.org/10.1016/j.cub.2019.10.015>.
- (25) Bröer, S.; Pauletti, A. Microglia and Infiltrating Macrophages in Ictogenesis and Epileptogenesis. *Front. Mol. Neurosci.* **2024**, *17*, 1404022. <https://doi.org/10.3389/fnMol.2024.1404022>.
- (26) Xiong, X.-Y.; Liu, L.; Yang, Q.-W. Functions and Mechanisms of Microglia/Macrophages in Neuroinflammation and Neurogenesis after Stroke. *Prog. Neurobiol.* **2016**, *142*, 23–44. <https://doi.org/10.1016/j.pneurobio.2016.05.001>.
- (27) Zhao, H.; Zhu, C.; Huang, D. Microglial Activation: An Important Process in the Onset of Epilepsy. *Am. J. Transl. Res.* **2018**, *10* (9), 2877–2889.
- (28) Iori, V.; Iyer, A. M.; Ravizza, T.; Beltrame, L.; Paracchini, L.; Marchini, S.; Cerovic, M.; Hill, C.; Ferrari, M.; Zucchetti, M.; Molteni, M.; Rossetti, C.; Brambilla, R.; Steve White, H.; D’Incalci, M.; Aronica, E.; Vezzani, A. Blockade of the IL-1R1/TLR4 Pathway Mediates Disease-Modification Therapeutic Effects in a Model of Acquired Epilepsy. *Neurobiol. Dis.* **2017**, *99*, 12–23. <https://doi.org/10.1016/j.nbd.2016.12.007>.
- (29) Liu, J.; Buisman-Pijlman, F.; Hutchinson, M. R. Toll-like Receptor 4: Innate Immune Regulator of Neuroimmune and Neuroendocrine Interactions in Stress and Major Depressive Disorder. *Front. Neurosci.* **2014**, *8*. <https://doi.org/10.3389/fnins.2014.00309>.
- (30) Mark, L. P.; Prost, R. W.; Ulmer, J. L.; Smith, M. M.; Daniels, D. L.; Strottmann, J. M.; Brown, W. D.; Hacein-Bey, L. Pictorial Review of Glutamate Excitotoxicity: Fundamental Concepts for Neuroimaging. *AJNR Am. J. Neuroradiol.* **2001**, *22* (10), 1813–1824.
- (31) Dong, X.; Wang, Y.; Qin, Z. Molecular Mechanisms of Excitotoxicity and Their Relevance to Pathogenesis of Neurodegenerative Diseases. *Acta Pharmacol. Sin.* **2009**, *30* (4), 379–387. <https://doi.org/10.1038/aps.2009.24>.
- (32) Berliocchi, L.; Bano, D.; Nicotera, P. Ca²⁺ Signals and Death Programmes in Neurons. *Philos. Trans. R. Soc. B Biol. Sci.* **2005**, *360* (1464), 2255–2258. <https://doi.org/10.1098/rstb.2005.1765>.
- (33) Chen, W.; Sheng, J.; Guo, J.; Gao, F.; Zhao, X.; Dai, J.; Wang, G.; Li, K. Tumor Necrosis Factor- α Enhances Voltage-Gated Na⁺ Currents in Primary Culture of Mouse Cortical Neurons. *J. Neuroinflammation* **2015**, *12* (1), 126. <https://doi.org/10.1186/s12974-015-0349-x>.

- (34) Rönnbäck, L.; Hansson, E. On the Potential Role of Glutamate Transport in Mental Fatigue. *J. Neuroinflammation* **2004**, *1* (1), 22. <https://doi.org/10.1186/1742-2094-1-22>.
- (35) Kumari, S.; Dhapola, R.; Sharma, P.; Nagar, P.; Medhi, B.; HariKrishnaReddy, D. The Impact of Cytokines in Neuroinflammation-Mediated Stroke. *Cytokine Growth Factor Rev.* **2024**, *78*, 105–119. <https://doi.org/10.1016/j.cytogfr.2024.06.002>.
- (36) Varvel, N. H.; Neher, J. J.; Bosch, A.; Wang, W.; Ransohoff, R. M.; Miller, R. J.; Dingledine, R. Infiltrating Monocytes Promote Brain Inflammation and Exacerbate Neuronal Damage after Status Epilepticus. *Proc. Natl. Acad. Sci.* **2016**, *113* (38). <https://doi.org/10.1073/pnas.1604263113>.
- (37) Bosco, D. B.; Tian, D.; Wu, L. Neuroimmune Interaction in Seizures and Epilepsy: Focusing on Monocyte Infiltration. *FEBS J.* **2020**, *287* (22), 4822–4837. <https://doi.org/10.1111/febs.15428>.
- (38) Strizova, Z.; Benesova, I.; Bartolini, R.; Novyzedlak, R.; Cecrdlova, E.; Foley, L. K.; Striz, I. M1/M2 Macrophages and Their Overlaps – Myth or Reality? *Clin. Sci.* **2023**, *137* (15), 1067–1093. <https://doi.org/10.1042/CS20220531>.
- (39) Hu, X.; Li, J.; Fu, M.; Zhao, X.; Wang, W. The JAK/STAT Signaling Pathway: From Bench to Clinic. *Signal Transduct. Target. Ther.* **2021**, *6* (1), 402. <https://doi.org/10.1038/s41392-021-00791-1>.
- (40) Philips, R. L.; Wang, Y.; Cheon, H.; Kanno, Y.; Gadina, M.; Sartorelli, V.; Horvath, C. M.; Darnell, J. E.; Stark, G. R.; O’Shea, J. J. The JAK-STAT Pathway at 30: Much Learned, Much More to Do. *Cell* **2022**, *185* (21), 3857–3876. <https://doi.org/10.1016/j.cell.2022.09.023>.
- (41) Sarapultsev, A.; Gusev, E.; Komelkova, M.; Utepova, I.; Luo, S.; Hu, D. JAK-STAT Signaling in Inflammation and Stress-Related Diseases: Implications for Therapeutic Interventions. *Mol. Biomed.* **2023**, *4* (1), 40. <https://doi.org/10.1186/s43556-023-00151-1>.
- (42) Remenyi, J.; Naik, R. J.; Wang, J.; Razsolkov, M.; Verano, A.; Cai, Q.; Tan, L.; Toth, R.; Raggett, S.; Baillie, C.; Traynor, R.; Hastie, C. J.; Gray, N. S.; Arthur, J. S. C. Generation of a Chemical Genetic Model for JAK3. *Sci. Rep.* **2021**, *11* (1), 10093. <https://doi.org/10.1038/s41598-021-89356-4>.
- (43) Cornejo, M. G.; Kharas, M. G.; Werneck, M. B.; Bras, S. L.; Moore, S. A.; Ball, B.; Beylot-Barry, M.; Rodig, S. J.; Aster, J. C.; Lee, B. H.; Cantor, H.; Merlio, J.-P.; Gilliland, D. G.; Mercher, T. Constitutive JAK3 Activation Induces Lymphoproliferative Syndromes in Murine Bone Marrow Transplantation Models. *Blood* **2009**, *113* (12), 2746–2754. <https://doi.org/10.1182/blood-2008-06-164368>.
- (44) McDonnell, M. E.; Bian, H.; Wrobel, J.; Smith, G. R.; Liang, S.; Ma, H.; Reitz, A. B. Anilino-Monindolylmaleimides as Potent and Selective JAK3 Inhibitors. *Bioorg. Med. Chem. Lett.* **2014**, *24* (4), 1116–1121. <https://doi.org/10.1016/j.bmcl.2014.01.001>.

- (45) Haan, C.; Rolvering, C.; Raulf, F.; Kapp, M.; Drückes, P.; Thoma, G.; Behrmann, I.; Zerwes, H.-G. Jak1 Has a Dominant Role over Jak3 in Signal Transduction through Γ c-Containing Cytokine Receptors. *Chem. Biol.* **2011**, *18* (3), 314–323. <https://doi.org/10.1016/j.chembiol.2011.01.012>.
- (46) Lv, Y.; Qi, J.; Babon, J. J.; Cao, L.; Fan, G.; Lang, J.; Zhang, J.; Mi, P.; Kobe, B.; Wang, F. The JAK-STAT Pathway: From Structural Biology to Cytokine Engineering. *Signal Transduct. Target. Ther.* **2024**, *9* (1), 221. <https://doi.org/10.1038/s41392-024-01934-w>.
- (47) Arter, C.; Trask, L.; Ward, S.; Yeoh, S.; Bayliss, R. Structural Features of the Protein Kinase Domain and Targeted Binding by Small-Molecule Inhibitors. *J. Biol. Chem.* **2022**, *298* (8), 102247. <https://doi.org/10.1016/j.jbc.2022.102247>.
- (48) Roskoski, R. Janus Kinase (JAK) Inhibitors in the Treatment of Neoplastic and Inflammatory Disorders. *Pharmacol. Res.* **2022**, *183*, 106362. <https://doi.org/10.1016/j.phrs.2022.106362>.
- (49) Taylor, S. S.; Keshwani, M. M.; Steichen, J. M.; Kornev, A. P. Evolution of the Eukaryotic Protein Kinases as Dynamic Molecular Switches. *Philos. Trans. R. Soc. B Biol. Sci.* **2012**, *367* (1602), 2517–2528. <https://doi.org/10.1098/rstb.2012.0054>.
- (50) Meharena, H. S.; Chang, P.; Keshwani, M. M.; Oruganty, K.; Nene, A. K.; Kannan, N.; Taylor, S. S.; Kornev, A. P. Deciphering the Structural Basis of Eukaryotic Protein Kinase Regulation. *PLoS Biol.* **2013**, *11* (10), e1001680. <https://doi.org/10.1371/journal.pbio.1001680>.
- (51) Hu, J.; Ahuja, L. G.; Meharena, H. S.; Kannan, N.; Kornev, A. P.; Taylor, S. S.; Shaw, A. S. Kinase Regulation by Hydrophobic Spine Assembly in Cancer. *Mol. Cell. Biol.* **2015**, *35* (1), 264–276. <https://doi.org/10.1128/MCB.00943-14>.
- (52) Lupardus, P. J.; Ultsch, M.; Wallweber, H.; Bir Kohli, P.; Johnson, A. R.; Eigenbrot, C. Structure of the Pseudokinase–Kinase Domains from Protein Kinase TYK2 Reveals a Mechanism for Janus Kinase (JAK) Autoinhibition. *Proc. Natl. Acad. Sci.* **2014**, *111* (22), 8025–8030. <https://doi.org/10.1073/pnas.1401180111>.
- (53) Saharinen, P.; Takaluoma, K.; Silvennoinen, O. Regulation of the Jak2 Tyrosine Kinase by Its Pseudokinase Domain. *Mol. Cell. Biol.* **2000**, *20* (10), 3387–3395. <https://doi.org/10.1128/MCB.20.10.3387-3395.2000>.
- (54) Ferrao, R.; Wallweber, H. J. A.; Ho, H.; Tam, C.; Franke, Y.; Quinn, J.; Lupardus, P. J. The Structural Basis for Class II Cytokine Receptor Recognition by JAK1. *Structure* **2016**, *24* (6), 897–905. <https://doi.org/10.1016/j.str.2016.03.023>.
- (55) Shan, Y.; Gnanasambandan, K.; Ungureanu, D.; Kim, E. T.; Hammarén, H.; Yamashita, K.; Silvennoinen, O.; Shaw, D. E.; Hubbard, S. R. Molecular Basis for Pseudokinase-Dependent Autoinhibition of JAK2 Tyrosine Kinase. *Nat. Struct. Mol. Biol.* **2014**, *21* (7), 579–584. <https://doi.org/10.1038/nsmb.2849>.

- (56) Glassman, C. R.; Tsutsumi, N.; Saxton, R. A.; Lupardus, P. J.; Jude, K. M.; Garcia, K. C. Structure of a Janus Kinase Cytokine Receptor Complex Reveals the Basis for Dimeric Activation. *Science* **2022**, 376 (6589), 163–169. <https://doi.org/10.1126/science.abn8933>.
- (57) Sun, S.; Rodriguez, G.; Zhao, G.; Sanchez, J. E.; Guo, W.; Du, D.; Rodriguez Moncivais, O. J.; Hu, D.; Liu, J.; Kirken, R. A.; Li, L. A Novel Approach to Study Multi-Domain Motions in JAK1's Activation Mechanism Based on Energy Landscape. *Brief. Bioinform.* **2024**, 25 (2), bbae079. <https://doi.org/10.1093/bib/bbae079>.
- (58) Wang, N.; Liang, H.; Zen, K. Molecular Mechanisms That Influence the Macrophage M1 and M2 Polarization Balance. *Front. Immunol.* **2014**, 5. <https://doi.org/10.3389/fimmu.2014.00614>.
- (59) Flanagan, M. E.; Blumenkopf, T. A.; Brissette, W. H.; Brown, M. F.; Casavant, J. M.; Shang-Poa, C.; Doty, J. L.; Elliott, E. A.; Fisher, M. B.; Hines, M.; Kent, C.; Kudlacz, E. M.; Lillie, B. M.; Magnuson, K. S.; McCurdy, S. P.; Munchhof, M. J.; Perry, B. D.; Sawyer, P. S.; Strelevitz, T. J.; Subramanyam, C.; Sun, J.; Whipple, D. A.; Changelian, P. S. Discovery of CP-690,550: A Potent and Selective Janus Kinase (JAK) Inhibitor for the Treatment of Autoimmune Diseases and Organ Transplant Rejection. *J. Med. Chem.* **2010**, 53 (24), 8468–8484. <https://doi.org/10.1021/jm1004286>.
- (60) Chrencik, J. E.; Patny, A.; Leung, I. K.; Korniski, B.; Emmons, T. L.; Hall, T.; Weinberg, R. A.; Gormley, J. A.; Williams, J. M.; Day, J. E.; Hirsch, J. L.; Kiefer, J. R.; Leone, J. W.; Fischer, H. D.; Sommers, C. D.; Huang, H.-C.; Jacobsen, E. J.; Tenbrink, R. E.; Tomasselli, A. G.; Benson, T. E. Structural and Thermodynamic Characterization of the TYK2 and JAK3 Kinase Domains in Complex with CP-690550 and CMP-6. *J. Mol. Biol.* **2010**, 400 (3), 413–433. <https://doi.org/10.1016/j.jmb.2010.05.020>.
- (61) Wang, Q.; Zorn, J. A.; Kuriyan, J. 5. Tofacitinib (Xeljanz™) Binds to a “DFG-in” Conformation of Janus Kinase. In *Protein kinase inhibitors in research and medicine*; Shokat, K., Ed.; Methods in enzymology; Elsevier/Academic Press: Amsterdam, 2014; p 41.
- (62) Rojas, A.; Banik, A.; Chen, D.; Flood, K.; Ganesh, T.; Dingleline, R. Novel Microglia Cell Line Expressing the Human EP2 Receptor. *ACS Chem. Neurosci.* **2019**, 10 (10), 4280–4292. <https://doi.org/10.1021/acscchemneuro.9b00311>.
- (63) Livak, K. J.; Schmittgen, T. D. Analysis of Relative Gene Expression Data Using Real-Time Quantitative PCR and the 2- $\Delta\Delta$ CT Method. *Methods* **2001**, 25 (4), 402–408. <https://doi.org/10.1006/meth.2001.1262>.
- (64) Zavoriti, A.; Miossec, P. Understanding Cardiovascular Events With JAK Inhibitors: Tofacitinib Reduces Synovial and Vascular Inflammation but Not the Prothrombotic Effects of Inflammatory Cytokines on Endothelium. *ACR Open Rheumatol.* **2025**, 7 (1), e11790. <https://doi.org/10.1002/acr2.11790>.

- (65) Park, B. S.; Lee, J.-O. Recognition of Lipopolysaccharide Pattern by TLR4 Complexes. *Exp. Mol. Med.* **2013**, *45* (12), e66–e66. <https://doi.org/10.1038/emm.2013.97>.
- (66) Helm, O.; Held-Feindt, J.; Grage-Griebenow, E.; Reiling, N.; Ungefroren, H.; Vogel, I.; Krüger, U.; Becker, T.; Ebsen, M.; Röcken, C.; Kabelitz, D.; Schäfer, H.; Sebens, S. Tumor-associated Macrophages Exhibit Pro- and Anti-inflammatory Properties by Which They Impact on Pancreatic Tumorigenesis. *Int. J. Cancer* **2014**, *135* (4), 843–861. <https://doi.org/10.1002/ijc.28736>.
- (67) Enz, L. S.; Zeis, T.; Schmid, D.; Geier, F.; Van Der Meer, F.; Steiner, G.; Certa, U.; Binder, T. M. C.; Stadelmann, C.; Martin, R.; Schaeren-Wiemers, N. Increased HLA-DR Expression and Cortical Demyelination in MS Links with HLA-DR15. *Neurol. Neuroimmunol. Neuroinflammation* **2020**, *7* (2), e656. <https://doi.org/10.1212/NXI.0000000000000656>.
- (68) Kwack, D. W.; Kim, D. W. The Increased Interleukin-6 Levels Can Be an Early Diagnostic Marker for New-Onset Refractory Status Epilepticus. *J. Epilepsy Res.* **2022**, *12* (2), 78–81. <https://doi.org/10.14581/jer.22015>.
- (69) Takashima, K.; Matsunaga, N.; Yoshimatsu, M.; Hazeki, K.; Kaisho, T.; Uekata, M.; Hazeki, O.; Akira, S.; Iizawa, Y.; Ii, M. Analysis of Binding Site for the Novel Small-molecule TLR4 Signal Transduction Inhibitor TAK-242 and Its Therapeutic Effect on Mouse Sepsis Model. *Br. J. Pharmacol.* **2009**, *157* (7), 1250–1262. <https://doi.org/10.1111/j.1476-5381.2009.00297.x>.
- (70) Svec, D.; Tichopad, A.; Novosadova, V.; Pfaffl, M. W.; Kubista, M. How Good Is a PCR Efficiency Estimate: Recommendations for Precise and Robust qPCR Efficiency Assessments. *Biomol. Detect. Quantif.* **2015**, *3*, 9–16. <https://doi.org/10.1016/j.bdq.2015.01.005>.
- (71) Taylor, S.; Wakem, M.; Dijkman, G.; Alsarraj, M.; Nguyen, M. A Practical Approach to q-PCR—Publishing Data That Conform to the MIQE Guidelines. *Methods* **2010**, *50* (4), S1–S5. <https://doi.org/10.1016/j.ymeth.2010.01.005>.
- (72) Netea, M. G.; Nold-Petry, C. A.; Nold, M. F.; Joosten, L. A. B.; Opitz, B.; Van Der Meer, J. H. M.; Van De Veerdonk, F. L.; Ferwerda, G.; Heinhuis, B.; Devesa, I.; Funk, C. J.; Mason, R. J.; Kullberg, B. J.; Rubartelli, A.; Van Der Meer, J. W. M.; Dinarello, C. A. Differential Requirement for the Activation of the Inflammasome for Processing and Release of IL-1 β in Monocytes and Macrophages. *Blood* **2009**, *113* (10), 2324–2335. <https://doi.org/10.1182/blood-2008-03-146720>.
- (73) McLachlan, J. A.; Serkin, C. D.; Bakouche, O. Dehydroepiandrosterone Modulation of Lipopolysaccharide-Stimulated Monocyte Cytotoxicity. *J. Immunol.* **1996**, *156* (1), 328–335. <https://doi.org/10.4049/jimmunol.156.1.328>.
- (74) Nakagawa, R.; Naka, T.; Tsutsui, H.; Fujimoto, M.; Kimura, A.; Abe, T.; Seki, E.; Sato, S.; Takeuchi, O.; Takeda, K.; Akira, S.; Yamanishi, K.; Kawase, I.; Nakanishi, K.; Kishimoto, T. SOCS-1 Participates in Negative Regulation of LPS Responses. *Immunity* **2002**, *17* (5), 677–687. [https://doi.org/10.1016/S1074-7613\(02\)00449-1](https://doi.org/10.1016/S1074-7613(02)00449-1).

- (75) Qin, H.; Roberts, K. L.; Niyongere, S. A.; Cong, Y.; Elson, C. O.; Benveniste, E. N. Molecular Mechanism of Lipopolysaccharide-Induced SOCS-3 Gene Expression in Macrophages and Microglia. *J. Immunol.* **2007**, *179* (9), 5966–5976. <https://doi.org/10.4049/jimmunol.179.9.5966>.
- (76) Kimura, A.; Naka, T.; Muta, T.; Takeuchi, O.; Akira, S.; Kawase, I.; Kishimoto, T. Suppressor of Cytokine Signaling-1 Selectively Inhibits LPS-Induced IL-6 Production by Regulating JAK–STAT. *Proc. Natl. Acad. Sci.* **2005**, *102* (47), 17089–17094. <https://doi.org/10.1073/pnas.0508517102>.
- (77) Sica, A.; Sacconi, A.; Borsatti, A.; Power, C. A.; Wells, T. N.; Luini, W.; Polentarutti, N.; Sozzani, S.; Mantovani, A. Bacterial Lipopolysaccharide Rapidly Inhibits Expression of C-C Chemokine Receptors in Human Monocytes. *J. Exp. Med.* **1997**, *185* (5), 969–974. <https://doi.org/10.1084/jem.185.5.969>.
- (78) Pérez-Baos, S.; Barrasa, J. I.; Gratal, P.; Larrañaga-Vera, A.; Prieto-Potin, I.; Herrero-Beaumont, G.; Largo, R. Tofacitinib Restores the Inhibition of Reverse Cholesterol Transport Induced by Inflammation: Understanding the Lipid Paradox Associated with Rheumatoid Arthritis. *Br. J. Pharmacol.* **2017**, *174* (18), 3018–3031. <https://doi.org/10.1111/bph.13932>.
- (79) Rosengren, S.; Corr, M.; Firestein, G. S.; Boyle, D. L. The JAK Inhibitor CP-690,550 (Tofacitinib) Inhibits TNF-Induced Chemokine Expression in Fibroblast-like Synoviocytes: Autocrine Role of Type I Interferon. *Ann. Rheum. Dis.* **2012**, *71* (3), 440–447. <https://doi.org/10.1136/ard.2011.150284>.
- (80) Ghoreschi, K.; Jesson, M. I.; Li, X.; Lee, J. L.; Ghosh, S.; Alsup, J. W.; Warner, J. D.; Tanaka, M.; Steward-Tharp, S. M.; Gadina, M.; Thomas, C. J.; Minnerly, J. C.; Storer, C. E.; LaBranche, T. P.; Radi, Z. A.; Dowty, M. E.; Head, R. D.; Meyer, D. M.; Kishore, N.; O’Shea, J. J. Modulation of Innate and Adaptive Immune Responses by Tofacitinib (CP-690,550). *J. Immunol.* **2011**, *186* (7), 4234–4243. <https://doi.org/10.4049/jimmunol.1003668>.
- (81) Bhagwat, S. S. Kinase Inhibitors for the Treatment of Inflammatory and Autoimmune Disorders. *Purinergic Signal.* **2009**, *5* (1), 107. <https://doi.org/10.1007/s11302-008-9117-z>.
- (82) Freeze, R.; Yang, K. W.; Haystead, T.; Hughes, P.; Scarneo, S. Delineation of the Distinct Inflammatory Signaling Roles of TAK1 and JAK1/3 in the CIA Model of Rheumatoid Arthritis. *Pharmacol. Res. Perspect.* **2023**, *11* (4), e01124. <https://doi.org/10.1002/prp2.1124>.
- (83) Ma, H.; Wang, C.; Han, L.; Kong, F.; Liu, Z.; Zhang, B.; Chu, W.; Wang, H.; Wang, L.; Li, Q.; Peng, W.; Yang, H.; Han, C.; Lu, X. Tofacitinib Promotes Functional Recovery after Spinal Cord Injury by Regulating Microglial Polarization via JAK/STAT Signaling Pathway. *Int. J. Biol. Sci.* **2023**, *19* (15), 4865–4882. <https://doi.org/10.7150/ijbs.84564>.
- (84) LaBranche, T. P.; Jesson, M. I.; Radi, Z. A.; Storer, C. E.; Guzova, J. A.; Bonar, S. L.; Thompson, J. M.; Happa, F. A.; Stewart, Z. S.; Zhan, Y.; Bollinger, C. S.; Bansal, P. N.; Wellen, J. W.; Wilkie, D. P.; Bailey, S. A.; Symanowicz, P. T.; Hegen, M.; Head, R. D.; Kishore, N.;

Mbalaviele, G.; Meyer, D. M. JAK Inhibition with Tofacitinib Suppresses Arthritic Joint Structural Damage through Decreased RANKL Production. *Arthritis Rheum.* **2012**, *64* (11), 3531–3542. <https://doi.org/10.1002/art.34649>.

(85) Yu, H.; Liu, Z.; Zhou, H.; Dai, W.; Chen, S.; Shu, Y.; Feng, J. JAK-STAT Pathway Modulates the Roles of iNOS and COX-2 in the Cytoprotection of Early Phase of Hydrogen Peroxide Preconditioning against Apoptosis Induced by Oxidative Stress. *Neurosci. Lett.* **2012**, *529* (2), 166–171. <https://doi.org/10.1016/j.neulet.2012.09.013>.

(86) Sareila, O.; Korhonen, R.; Kärpäniemi, O.; Nieminen, R.; Kankaanranta, H.; Moilanen, E. JAK Inhibitors AG-490 and WHI-P154 Decrease IFN-Gamma-Induced iNOS Expression and NO Production in Macrophages. *Mediators Inflamm.* **2006**, *2006* (2), 16161. <https://doi.org/10.1155/MI/2006/16161>.

(87) Weber, A.; Wasiliew, P.; Kracht, M. Interleukin-1 (IL-1) Pathway. *Sci. Signal.* **2010**, *3* (105). <https://doi.org/10.1126/scisignal.3105cm1>.

(88) Hendrayani, S.-F.; Al-Harbi, B.; Al-Ansari, M. M.; Silva, G.; Aboussekhra, A. The Inflammatory/Cancer-Related IL-6/STAT3/NF- κ B Positive Feedback Loop Includes AUF1 and Maintains the Active State of Breast Myofibroblasts. *Oncotarget* **2016**, *7* (27), 41974–41985. <https://doi.org/10.18632/oncotarget.9633>.

(89) Dinarello, C. A. Interleukin-1 in the Pathogenesis and Treatment of Inflammatory Diseases. *Blood* **2011**, *117* (14), 3720–3732. <https://doi.org/10.1182/blood-2010-07-273417>.

(90) Muzio, M.; Natoli, G.; Sacconi, S.; Levrero, M.; Mantovani, A. The Human Toll Signaling Pathway: Divergence of Nuclear Factor κ B and JNK/SAPK Activation Upstream of Tumor Necrosis Factor Receptor–Associated Factor 6 (TRAF6). *J. Exp. Med.* **1998**, *187* (12), 2097–2101. <https://doi.org/10.1084/jem.187.12.2097>.

(91) Okugawa, S.; Ota, Y.; Kitazawa, T.; Nakayama, K.; Yanagimoto, S.; Tsukada, K.; Kawada, M.; Kimura, S. Janus Kinase 2 Is Involved in Lipopolysaccharide-Induced Activation of Macrophages. *Am. J. Physiol.-Cell Physiol.* **2003**, *285* (2), C399–C408. <https://doi.org/10.1152/ajpcell.00026.2003>.

(92) Beurel, E.; Joep, R. S. Lipopolysaccharide-Induced Interleukin-6 Production Is Controlled by Glycogen Synthase Kinase-3 and STAT3 in the Brain. *J. Neuroinflammation* **2009**, *6* (1), 9. <https://doi.org/10.1186/1742-2094-6-9>.

(93) Minogue, A. M.; Barrett, J. P.; Lynch, M. A. LPS-Induced Release of IL-6 from Glia Modulates Production of IL-1 β in a JAK2-Dependent Manner. *J. Neuroinflammation* **2012**, *9* (1), 629. <https://doi.org/10.1186/1742-2094-9-126>.

(94) Dang, B.; Gao, Q.; Zhang, L.; Zhang, J.; Cai, H.; Zhu, Y.; Zhong, Q.; Liu, J.; Niu, Y.; Mao, K.; Xiao, N.; Liu, W.-H.; Lin, S.; Huang, J.; Huang, S. C.-C.; Ho, P.-C.; Cheng, S.-C. The

Glycolysis/HIF-1 α Axis Defines the Inflammatory Role of IL-4-Primed Macrophages. *Cell Rep.* **2023**, 42 (5), 112471. <https://doi.org/10.1016/j.celrep.2023.112471>.

(95) Lee, Y. W.; Lee, W. H.; Kim, P. H. Oxidative Mechanisms of IL-4-Induced IL-6 Expression in Vascular Endothelium. *Cytokine* **2010**, 49 (1), 73–79. <https://doi.org/10.1016/j.cyto.2009.08.009>.

(96) Villarino, A. V.; Gadina, M.; O'Shea, J. J.; Kanno, Y. SnapShot: Jak-STAT Signaling II. *Cell* **2020**, 181 (7), 1696-1696.e1. <https://doi.org/10.1016/j.cell.2020.04.052>.

(97) Zareifard, A.; Beaudry, F.; Ndiaye, K. Janus Kinase 3 Phosphorylation and the JAK/STAT Pathway Are Positively Modulated by Follicle-Stimulating Hormone (FSH) in Bovine Granulosa Cells. *BMC Mol. Cell Biol.* **2023**, 24 (1), 21. <https://doi.org/10.1186/s12860-023-00482-5>.

(98) Yang, L.; Huh, J. R.; Choi, G. B. One Messenger Shared by Two Systems: How Cytokines Directly Modulate Neurons. *Curr. Opin. Neurobiol.* **2023**, 80, 102708. <https://doi.org/10.1016/j.conb.2023.102708>.

(99) Conti, B.; Tabarean, I.; Sanchez-Alavez, M.; Davis, C.; Brownell, S.; Behrens, M.; Bartfai, T. Cytokine Receptors in the Brain. In *NeuroImmune Biology*; Elsevier, 2008; Vol. 6, pp 19–38. [https://doi.org/10.1016/S1567-7443\(07\)10002-8](https://doi.org/10.1016/S1567-7443(07)10002-8).